Master of Science Thesis

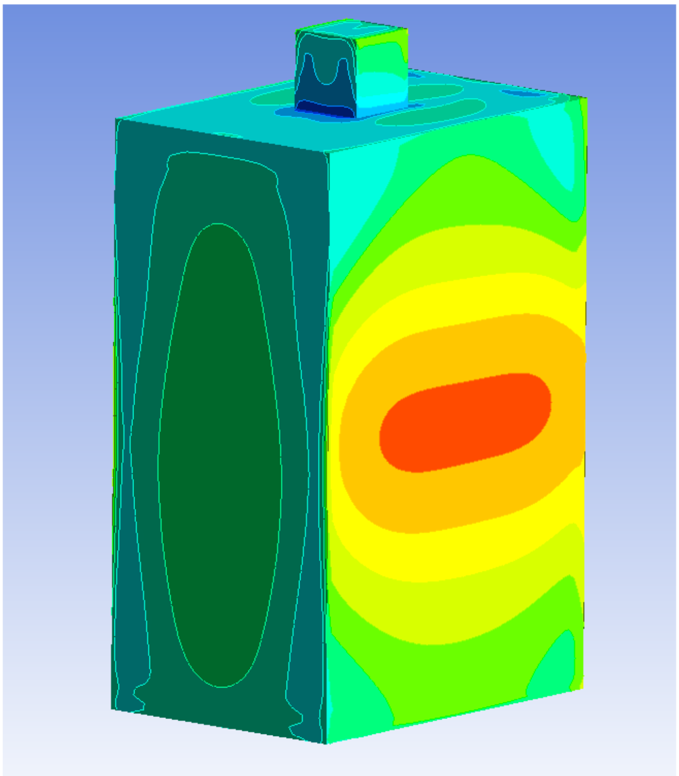

Shrink Sleeve Labeling

Fundamental understanding of heat transfer due to the flow field

Gert-Jan Noben

October 29, 2014

Faculty of Aerospace Engineering

Delft University of Technology

Shrink Sleeve Labeling

Fundamental understanding of heat transfer due to the flow field

Master of Science Thesis

For obtaining the degree of Master of Science in Aerospace Engineering
at Delft University of Technology

Gert-Jan Noben

October 29, 2014

Faculty of Aerospace Engineering · Delft University of Technology

Delft University of Technology

DELFT UNIVERSITY OF TECHNOLOGY
DEPARTMENT OF AERODYNAMICS

The undersigned hereby certify that they have read and recommend to the Faculty of Aerospace Engineering for acceptance the thesis entitled **"Shrink Sleeve Labeling"** by **Gert-Jan Noben** in fulfillment of the requirements for the degree of **Master of Science**.

Dated: October 29, 2014

Supervisors:

Dr. ir. B. W. van Oudheusden

Dr. ir. A.H. van Zuijlen

Dr. ir. M. Pini

Summary

In this thesis the goal is to grow the fundamental understanding of the Shrink Sleeve Labeling process, specifically on the steam tunnel equipment. The research is focused on the heat transfer phenomena of the flow on to the bottle. From literature was found that the problem could be split into 3 general domains: 1) free jet flow, 2) heat transfer by impinging jet and 3) condensation heat transfer. The condensation part was seen as an optional part since it would have a big impact on the way the numerical model will be setup. This thesis therefore is setup to handle the free jet flow and heat transfer by an impinging jet.

To investigate the flow it is chosen to build a numerical tool that can simulate the flow properties and its heat transfer to a bottle that is transported through the flow. The numerical tool is setup in ANSYS Fluent in a step-wise method by simulating 1) the smallest free jet flow properties 2) the heat transfer properties of the impinging free jet 3) a specific steam nozzle flow with its heat transfer properties and finally 4) a full steam tunnel flow with multiple nozzles and a moving bottle. The main subjects of the investigation are to select a turbulence model that accurately predicts the free jet flow, to select wall functions or wall treatments for correctly resolving the boundary layer flow on the bottle, to design a mesh that can calculate all gradients in the flow but also allows for cheap computational efforts and finally to build a set of results that can be validated with measurements. The assumptions with most impact made in this model are that condensation is not simulated which therefore neglects the latent heat that comes free in the tunnel and on the bottle and a geometrical simplification is made for cheaper computational effort.

To gather inputs for the boundary conditions of the models and to perform measurements for the validation of the model, an experiment was done on real steam tunnel. Measurements were done in collaboration with P&G's steam tunnel supplier Fuji Seal.The first set of measurements gather steam pressures, temperatures and flow rates in the supply system for different settings of the tunnel. They are used to specify the nozzle steam conditions which are the main driver of the jet flow. A second set of measurements is done with a so-called "SMART-bottle"©that was specially designed for measuring the temperatures seen by a bottle that is transported through the tunnel. It was used to measure the temperatures of different settings, giving an insight in the correlations between the settings and what the bottle experiences. Settings ran with the SMART-bottle are simulated with the final model and used as a validation of the model.

For validation purposes the final full scale model was based on the dimensions on a Fuji Seal steam tunnel. Because the modelling basis for different shrink sleeve tunnel dimensions and for different bottle shapes will stay the same, we can say that this was a general research in shrink sleeve labeling flow dynamcis that can be broadly applied. The only changes needed for simulating other steam tunnels are updating the geometry , the mesh should be detailed according the new geometry and the inlet and outlet boundary conditions should be recalculated.

What could be concluded from this research are: 1) the final model is able to give good fundamental insights in the flow and heat transfer properties of the steam tunnels. Taking into account its assumptions, the results are within a reasonable error margin from the measurements which gives confidence that the simulations are correct. 2) Using the $k - \epsilon$ realizable turbulence model together with enhanced wall treatments are a viable option for modeling the flow and heat transfer properties of shrink sleeve labelling process. The simulation of a full case now take around 5 days to be calculated, which is a computational expensive effort. 3) This model does give the opportunity to be used as a resource for setting up an empirical model that shows the relation between for example the flow rate at the nozzles and the expected heat taken by a bottle. This would be a next step after this research 4) From nozzle simulations can be concluded that the variables with most impact on the heat transfer are the distance from the jet exit to the bottle and the flow rate through the nozzle. The geometry of the nozzles have less impact then originally expected.

In the next chapters the introduction to the research and its back ground are explained, further the full design approach of the model is treated, results of the models and measurements are presented together with a validation.

Acknowledgements

First of all I would like to thank Yann Healy, Maneesh Adyanthaya, Julio Muniz and Vito Gomes for giving me the opportunity to do my internship and thesis work at Procter & Gamble and for their support, guidance and patients during my time at BIC. Especially I thank Maneesh for helping me setup the experiments at Fuji Seal which was one of the greater experiences of my internship and for sharing your experiences during the car-rides between Brussel and Deurne. Also I thank Yann for his many inputs and patience while I was learning to work with Fluent and trying to puzzle out the post-processing. I would like to thank Dr. Sander van Zuijlen for his support and feedbacks at the TU Delft, for being very reachable during my internship and for investing all his valuable time for meetings when I was back in Delft.Of course I would like to thank all my friends for listening to the many shrink sleeve labelling stories, for their encouragements and being understanding during the busy times. I thank my family for their support during the whole of my studies and staying behind me until the finish. And last but not least, I thank Jasmijn for her love and care!

Table of Contents

List of Figures

Chapter 1

Introduction

In this research, a start is made on the development of a computational tool that represents the flow and heat transfer characteristics of Shrink Sleeve Labelling process. This research will be done with support and financing of Procter & Gamble (P&G) in Brussels. P&G is an American multinational consumer goods company which focuses on fabric care, home care, health care, baby- and feminine care and beauty products. In their Global Modeling & Simulation department, P&G focuses on assisting the business with computer models that help engineers understand the processes, equipment, material behaviour, etc. which they use in manufacturing and also how the products perform at the consumer. Within this department there is a group M&S packaging that has its focus on the packages of the products. Here the research on Shrink Sleeve Labelling will be done.

In this chapter the background of the process and the incentive for developing the computational tool is explained.

1.1 Background Shrink Sleeve Labeling

Shrink Sleeve Labelling is currently one of the premium types of package decorations. The reason for this is that it can have a 360 degree and top to bottom coverage of the package, which is unique comparing to other labelling techniques. Consumer ratings of shrink sleeved packages are high, therefore many companies are investing in these labels for the premium segments of their products. Cost-wise it has similar equipment cost, but a multiple in reoccurring material cost.

The labels, also called sleeves because of there shape, are made of certain types of plastics who have a shrinking behaviour because of their manufacturing process. The shrinking is driven by heating the sleeve, which will make it form itself 360 degrees around the shape of the bottle. More details follow in the upcoming chapter.

The application of shrink sleeves on bottles done through 2 stages. See figure 1.1. First the sleeve is thrown over a bottle. This is done with a so called sleeve-applicator, which will not be further explained since it is out of the scope of this thesis. Second, heat is added to the sleeve so it will shrink around the contours of the bottle in a shrink-tunnel, further also called the steam tunnel. The heating process can also be done with other types of machinery, namely hot-air tunnels or infra-red tunnels. This thesis will focus on the steam tunnel, since this was the main interest of P&G . Examples of a steam-tunnels can be seen in fig. 1.2.

Figure 1.1: Shrink sleeve application graphical

Figure 1.2: Examples of steam tunnels: Quadrel Systems (2014), Sleeve Seal Houston (2014) and Axon Axon (2014)

The incentive from P&G for this research is to grow their fundamental understanding of the steam tunnel by studying the physics happening inside the tunnel. Currently the operating windows of a steam tunnel for new shrink sleeve labeling initiatives are defined by trail and error testing. This is a very time and resource consuming method to find good equipment settings. Since shrink sleeving is such a complex process, experience with the machinery is key to find the settings. Therefore a lot of knowledge is held by the the operators at the supplier and operators in the plant. When new tunnels are to be acquired or when changes in existing production lines are about to happen, the operating windows of the tunnel need to be found and proven through a test project in collaboration with the supplier. P&G therefore is looking for more fundamental understanding of the process and of the current tunnel which should give insights that help with predicting equipment settings, help with defining the critical transformations in the process that need to be tested, and thereby decreasing risks for startups of new initiatives and also shortening test projects. This thesis will focus on the fluid

To better understand the process and its critical parameters, in the following sections more details will be described on the Bottles & Labels, the Machinery, etc.

1.2 Bottles and Labels

Shrink Sleeve Labelling is most commonly used for labelling bottles and for bundling multiple bottles. Sleeve materials are made of PET, PVC, PLA and OPS, which are all thermoplastic materials. To give the sleeves their shrinking properties, a series of extruding and stretching is used in the manufacturing process. Because of the thermoplastic behaviour of the materials, when heat is added they have the tendency to return back to their original shape. This is the physical phenomena that drives the shrinking of a sleeve. During the stretching process, directions in which the sleeve will shrink can be given. The circumferential shrink will most often be maximised and the longitudinal shrink will be minimised. This will give the sleeve the tendency to nicely shrink around a bottle, without shortening from top to bottom. Other variables of the sleeves are the thickness of the sleeve, typically ranging from 30 micron to 70 micron. Also the density can change, which makes it possible to recycle the PET sleeve separate from the PET bottle. Examples can be seen in graphs 1.3 and 1.4

In the consumer goods sector the most often used material for bottles is PET which is a good workable material, it is transparent and is recyclable. For shrink sleeve material there are many options with all their own advantages and disadvantages. The critical criteria are shrink ratio, which is the lenght-percentage that the material has shrinked after heating, the transparency, the machinability and the recyclability.

For this research it is interesting to focus on the heat transport between the flow and a PET sleeve with PET bottle. Since the material properties such as the specific heat, density, etc, are very similar for the PET bottle and PET sleeve, they will show the same shrink characteristics. Of course the bottle should not deform and the sleeve should be fully deformed, which makes this a challenging case. Therefor in all numerical-models of this thesis where heat transfer is simulated, the wall properties will be based on PET.

Figure 1.3: Shrink sleeve label: P&G

Figure 1.4: Shrink sleeve label examples

1.3 Machinery

1.3.1 Tunnel

The hull of steam tunnels in general are designed to enclose the full heating process, mainly to keep steam from leaving the system for safety reasons and to keep heat inside for efficiency. Examples of different steam tunnels are shown in figures 1.2 In side the tunnel, bottles with a sleeve are transported over a conveyor belt such that the heat from the fluid in the tunnel can be transported with as goal to make the sleeve shrink. The steam is supplied with a

1.3.2 Steam supply system

In general a branching of pipes will supply steam from a boiler to the places in the tunnel where it is sprayed on the bottles with some kind of nozzle. All manufactures have their own way of bringing steam to the nozzles and have their specific design of nozzles. Manufacturers want their tunnels to be versatile so that many different bottles sizes and shapes can be sleeved. To make this possible, the flow rates of the steam is should be adjustable at different locations in the tunnel. This results in the fact that steam supply systems can become complex piping and valve systems that should be taken into account when trying to understand the shrink sleeve machinery. A general example of a piping and valve system can be seen in figure 1.5.

1.3.3 Nozzles

To spray steam on the bottles that move through the tunnel, so called nozzles are used. The main goal of the nozzles is to direct the steam to the bottles in a controlled manner. Nozzles are generally positioned at both sides of the conveyor belt which ensures a symmetrical heat distribution on the bottle. The nozzle distance relative to the conveyor belt are often adjustable, together with the height and angle to compose settings for sleeving different sizes and shapes of bottles. Valves in the steam supply system will regulated the throughput of the nozzles. A couple of examples are seen in the sketches below, graphs 1.7. The nozzles

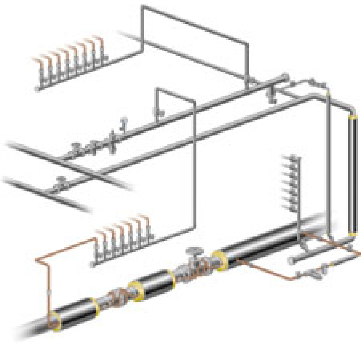

Figure 1.5: General steam supply example

used in the tunnel that was available for the experiment of this thesis are taken as a basis of the sketches. These nozzles are box-shaped pressure headers with different sizes and shapes of holes to spray the steam outside.

Figure 1.6: Nozzles inside steam tunnel

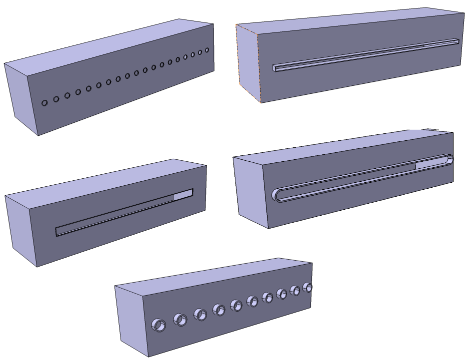

Figure 1.7: Catia sketches of example nozzles

1.3.4 Exhaust

On the shrink sleeve tunnels an exhaust system will be installed to extract the steam that enters the tunnel via the nozzles. Since no steam may leave the tunnel, these exhaust system's extraction rates are higher than the inflow rate of steam. The exhaust is often used as a regulator for average temperature of the tunnel, so it will influence the heat seen by a bottle. An example of the exhaust can be seen on the top of Quadrel steam tunnel in figure 1.2.

1.4 Problem statement

The goal of this research will be to investigate the heat transfer phenomena from the steam flow to the sleeve and bottle in Shrink Sleeve Labeling tunnels. Since the heat taken by the sleeve will be triggering the shrink process, this will be the main parameter to focus. From P&G the purpose was articulated:

"Drive fundamental understanding of the steam tunnel equipment". It is focused on 1) the impact of the settings on the flow and 2) the impact of the settings on the sleeves and bottles. This thesis will focus on the flow and heat transfer part of the process. Which means that the shrinking of the label, so the structural part of the process is neglected. An understanding of the capabilities of the current equipment needs to be built. And thereafter we need to learn what the impact is of all the input variables on the output. This output should look like an energy or temperature profile that is seen by a bottle which travels through the steam tunnel. On a broader scope, if we can understand how the current equipment works and what it's operating conditions are, the next goal is to research what the impact of changes on the equipment would be on the heat profile of the bottle.

From the literature part of the research is found that the flow and heat transfer phenomena to be understood can be split up into 3 domain: 1) free jet flow, 2) heat transfer by impinging jet and 3) condensation heat transfer. From the start, the condensation part was seen as an optional part since it would have a big impact on the way the numerical model will be setup. This thesis therefore is setup to handle the free jet flow and heat transfer by an impinging jet.

For the free jet flow and heat transfer by the impinging jet, an investigation will be done into which turbulence model that will be used, the development of the mesh will be researched to allow for good results and the boundary conditions of the nozzles and extraction fan need to be investigated. Defining the turbulence model will be based on the theory part in this thesis and on test-cases with different models. The mesh development will be performed according guidelines of Fluent tutorials and checked with a mesh sensitivity analysis. The boundary conditions and validation data will be gathered during an experimental research on a steam tunnel and on bottles inside the tunnel. These experiments were an integral part of the thesis work.

Since their is a lack of data on the input conditions of the steam in the steam tunnel, experimental measurements need to be performed. An understanding of the steam properties at the nozzles needs to be found and also the extraction fan and conveyor inlet and outlet flow velocities need to be understood. Finally, for validation of the numerical model, measurement should be performed for the heat transfer of the flow to the bottle. With this data a comparison between the numerical data and experimental data can be made.

Chapter 2

Theory

From the problem statement, the goal is set to first simulate the impinging jet heat transfer of the tunnel. It consist of 3 main features that need to be captured by the model. First the jet flow from the nozzle, second the wall flow on the impingement wall and third the heat transfer on the impingement wall.

Setting up the CFD model contains several steps: an investigation what is the impact of turbulence models, wall functions, boundary conditions and research the density of the geometry mesh.

2.1 Submerged jet flow and wall flow

To check the results of our model, data from papers like Boguslawski and Popiel (1979) and Behnia et al. (1997) are used as references for the flow structure of the jet and heat transfer to on the impinging wall. When looking for a way to validate the characteristics of jet flows, the following basic principles are followed.The diameter of the nozzle opening is used as a reference value D. Some general characteristics coming from literature are: at a distance of 6 diameters downstream of the nozzle exit, z/D = 6, the mean longitudinal velocity on the jet centre line starts to rapidly increase. See figure 2.2. Between z/D = 4 and 9 the turbulence intensity on the jet centre line rapidly increases, whereafter it keeps slowly increasing further downstream.

The goal of this first section is to define how the impinging nozzle jets can be simulated. First the focus will be to find out which RANS turbulence model will be suitable. It will need to accurately solve the Nusselt number on the impinging wall. Next to the turbulence model, also the mesh should be designed in a proper way and the boundary conditions need to be determined.

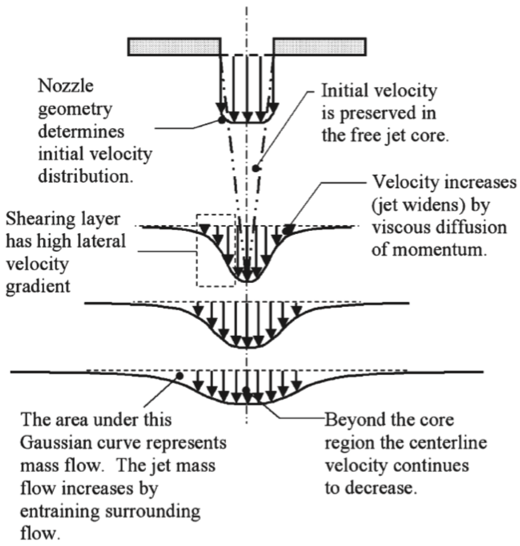

Figure 2.1: Submerged impinging jet flow field

The focus areas for correctly modelling the impinging jets are the free jet flow field, see figure 2.1 and the impinging region, see figure 2.3. The flow field will be characterised by the jet angle, the jet core length and the velocities. From a physical point of view the shape of the nozzle, the upstream turbulence intensity and the pressure delta over the nozzle will influence the drivers of the flow field.

Structure of the free round turbulent jet **535**

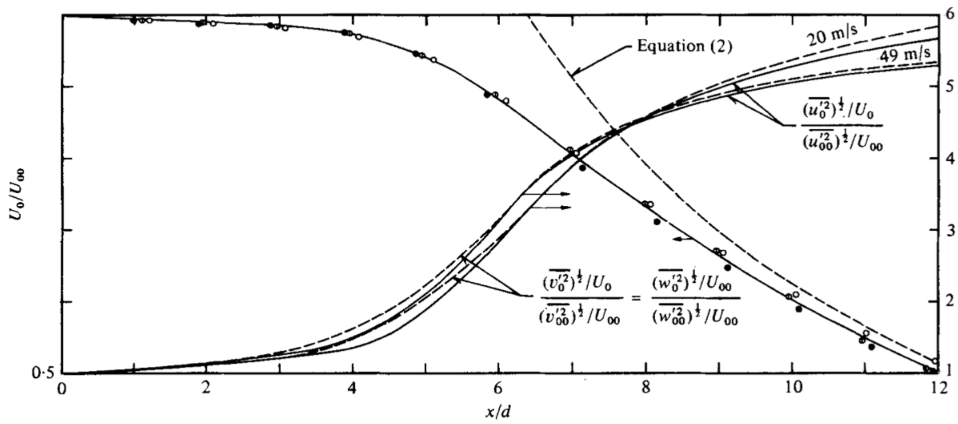

FIGURE 6. Axial variation of the longitudinal mean velocity and relative turbulent intensities on the jet centre-line. ○, $U_{00} = 20\,\mathrm{m/s}$; ⦶, $U_{00} = 30\,\mathrm{m/s}$; ●, $U_{00} = 49\,\mathrm{m/s}$. $\overline{(u'^2)}^{\frac{1}{2}}/U_{00} = 3{\cdot}8 \pm 0{\cdot}1\,\%$,

Figure 2.2: Axial mean velocity and turbulent intensities of jet centre line

In the middle of the impacting jet at the wall, a stagnation point will arise. Around the stagnation region, the flow will be bend outward and create a wall flow. The difficulty for modelling lays in the boundary layer flow at the wall. It is influenced by the velocities in the flow field, the turbulence of the jet flow and the roughness of the wall.

For the heat transfer of the jet to the wall, the important parameters to model are the

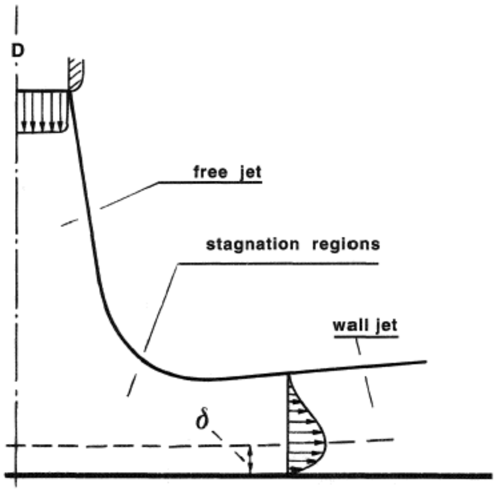

Figure 2.3: Submerged impinging jet shape

boundary layer flow. This influences the velocity profile and the temperature profile of the wall flow. Further, the heat transfer characteristics of the wall and the fluid will be important, therefore the material characteristics and temperatures are important. Empirical relations of the Nusselt number, which will be shortly explained in sections 3 with equation (3.4), are always dependent on the Reynolds number and Prandtl number. These show respectively the ratio between inertia and viscous forces in a flow and the ratio of momentum diffusivity and thermal diffusivity.

2.2 Turbulence modeling and Wall functions

Turbulent flows are characterised by velocity fluctuations in all directions and has an infinite number of degrees of freedom. Since the flow is 3D, chaotic, diffusive, dissipative and intermittent, it is almost impossible to find a solution for the full Navier Stokes equations. Therefore different types of turbulent modelling are used to overcome this complexity. References used in the following section are TU Delft lectures notes "Turbulence A" and Nieuwstadt (1992)

2.2.1 Direct Numerical Simulation

To be able to solve all the scales of the turbulent flow so that a total numerical resolution of the flow is constructed,Direct Numerical Simulation (DNS), a grid is needed with a number of nodes proportional to $Re^{9/4}$. The high amount of grid nodes needs a high memory storage. In addition, the time intervals to be able to simulate the the turbulence time scale is proportional to $Re^{3/4}$. This combination means that a high computational cost will be needed, even for low Reynolds number problems.

The governing equations for a Newtonian fluid are: Conservation of Mass

$$\frac{\partial \rho}{\partial t} + \frac{\partial \rho \tilde{u}_i}{\partial x_i} = 0 \tag{2.1}$$

Conservation of momentum

$$\frac{\partial \rho \tilde{u}_i}{\partial \tau} + \frac{\partial \rho \tilde{u}_j \tilde{u}_i}{\partial x_j} = \frac{\partial}{\partial x_j}\left(\mu \frac{\partial \tilde{u}_i}{\partial x_j}\right) - \frac{\partial \tilde{p}}{\partial x_i} + \rho g_i + \tilde{s}_{ui} \tag{2.2}$$

Conservation of passive scalars ($\tilde{T}$)

$$\frac{\partial \rho c_p \tilde{T}}{\partial \tau} + \frac{\partial \rho c_p \tilde{u}_j \tilde{T}}{\partial x_j} = \frac{\partial}{\partial x_j}\left(k \frac{\partial \tilde{T}}{\partial x_j}\right) + \tilde{s}_t \tag{2.3}$$

2.2.2 Reynolds Averaged Nasvier Stokes

One solution for this problem is reducing the scales by using Reynolds decompositions. It means that a split-up is made, for any property, of the average value and its fluctuating part. e.g. for the flow speed,

$u(x, y, z, t) = \overline{u(x, y, z)} + u'(x, y, z, t)$

Where $\overline{u}$ represents the mean flow speed and u' the fluctuations over time.The fluctuations are so that their time average equal zero. The new equations will be exact for an average flow field, but not for the exact turbulent flow field, which are called the Reynolds Averaged Navier Stokes Equations (RANS).

Conservation of Mass

$$\frac{\partial \rho}{\partial t} + \frac{\partial \rho \overline{u_i}}{\partial x_i} = 0 \tag{2.4}$$

Conservation of momentum

$$\frac{\partial \rho \overline{u_i}}{\partial \tau} + \frac{\partial \rho \overline{u_j} \overline{u_i}}{\partial x_j} = \frac{\partial}{\partial x_j}\left(\mu \frac{\partial \overline{u_i}}{\partial x_j} - \rho \overline{u_i' u_j'}\right) - \frac{\partial \overline{p}}{\partial x_i} + S_{ui} \tag{2.5}$$

Conservation of passive scalars ($\tilde{T}$)

$$\frac{\partial \rho c_p \overline{T}}{\partial \tau} + \frac{\partial \rho c_p \overline{u_j} \overline{T}}{\partial x_j} = \frac{\partial}{\partial x_j}\left(k \frac{\partial \overline{T}}{\partial x_j} - \rho c_p \overline{u_j t}\right) + S_t \tag{2.6}$$

By adapting the NS-equations, new unknowns are introduced. We add 9 unknowns which are 6 turbulent stresses and 3 turbulent fluxes. Turbulence Modelling will provide for the additional equations to model the unknowns, or multiple PDE's for the turbulent stresses and fluxes will be used to guide the modelling.

In order of increasing complexity one can use:

- Algebraic models: mixing length (first order model)
- 1 equation models: k-model, μ_t-model (first order model)
- 2 equation models: $k-\epsilon$, $k-kl$, $k-\omega^2$, low Re$k-\epsilon$ (first order model)
- Algebraic stress models: ASM (second order model)
- Reynolds stress models: RSM (second order model)

First order models are based on the analogy between laminar and turbulent flows, which are called Eddy Viscosity Models. They are setup such that the average turbulent flow field is similar to a corresponding laminar flow. This analogy is referred to as the Boussinesq hypothesis. In Beer (2012) a good introduction is given on the mixing-length hypothesis. For laminar flows:

$$\tau_{ij} = \mu \left(\frac{\partial u_i}{\partial x_j} + \frac{\partial u_j}{\partial x_i} \right) - \frac{2}{3}\mu\delta_{ij}\frac{\partial u_j}{\partial x_j} \tag{2.7}$$

$$q_i = \frac{k}{c_p}\frac{\partial T}{\partial x_i} \tag{2.8}$$

For turbulent:

$$\tau_{ij}^t = \rho\overline{u_i u_j} = \mu_t \left(\frac{\partial U_i}{\partial x_j} + \frac{\partial U_j}{\partial x_i} \right) - \frac{2}{3}\delta_{ij}\rho k \tag{2.9}$$

$$q_i^t = -\rho\overline{u_i t}\frac{k_t}{c_p}\frac{\partial T}{\partial x_i} \tag{2.10}$$

, where μ_t is the Turbulent Viscosity, k is the Turbulent Kinetic Energy and k_t is the Turbulent Conduction Coefficient. These coefficient are flow properties, who will be used to find the turbulent stresses and fluxes.

In *one-equation models*, which is the k-model a PDE is derived for the kinetic energy. The turbulent viscosity and conduction coefficient will be expressed as a function of the turbulent kinetic energy.

For *two-equation models* two PDE's are derived, e.g. for the $k-\epsilon$ model one equation for the turbulent kinetic energy (k) and one for the turbulent dissipation rate (ϵ). The PDE for the turbulent kinetic energy is obviously the same as for the k-model. The turbulent viscosity will be derived as a function of both factors, k and ϵ.

Second Order Models are setup to make use of the governing equations for the second order moments, Reynolds stresses and turbulent fluxes, instead of the Boussinesq hypothesis. These models will be better in dealing with the anisotropy of turbulence and the extra strains. Comparing to first order models it has a large number of PDE's. The most used models are the Algebraic Stress Model and Reynolds Stress Model.

2.2.3 Large Eddy Simulation

Another solution for the amount of scales is the Large Eddy Simulation (LES) which tracks down flow properties with the full equations to a specific user defined length scale, and then uses additional equations who act on a smaller length scale to describe its turbulent flow behaviour. Since it still uses the full NS-equations for a large part of the flow, it is computational costly method and is mainly used for problems with $Re < 1000$.

2.2.4 Wall functions

Flows are greatly affected by the presence of walls, especially the velocity field, but also the turbulence and energy of the flow will change. Modelling these near-wall effects will be important to give a good prediction of the heat transfer between the jet flows and the impinging wall. From White and Corfield (1991) we know that the near-wall region can be divided into 3 layers. The layer closest to the wall is called the viscous sublayer, which is almost laminar and where viscosity plays a dominant role in momentum, heat and mass transfer. The layer furthest away from the wall is called the fully-turbulent-layer where turbulence has the biggest impact on the flow. In between these 2 layers, the molecular viscosity and turbulence both have equal impact. See figure 2.4 for a visual representation.

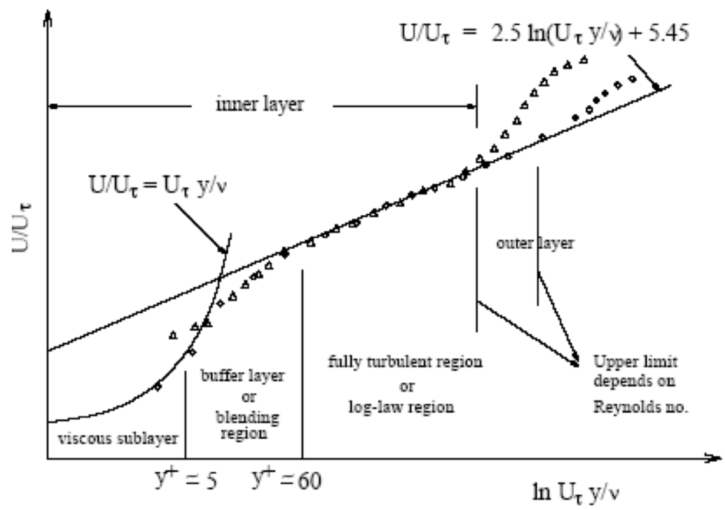

Figure 2.4: Wall functions: Near-wall subdivision

Here y^+ is defined as follows:

$$y^+ = yv^*/\nu \tag{2.11}$$

$$v^* = (\tau_w/\rho)^{1/2} \tag{2.12}$$

To numerically solve the near wall region, there are 2 options. 1) the viscous sublayer will not be resolved, but a so called wall function is used to represent the flow between the wall and the fully-turbulent layer. Wall functions are semi-empirical equations that represent the algorithmic boundary layer, there for there is no need for a dense mesh. 2) the mesh is very fine on the wall, so the turbulence model can resolve the flow until the viscous sublayer. Fluent provides both approaches.

Equations for wall functions

For resolving momentum, the wall functions consist of the following equations, also known as the Law-of-the-wall:

$$U^* = \frac{1}{\kappa} ln\left(Ey^*\right) \tag{2.13}$$

$$U^* = \frac{U_P C_\mu^{1/4} k_P^{1/2}}{\tau_w/\rho} \tag{2.14}$$

$$y^* = \frac{\rho C_\mu^{1/4} k_P^{1/2} y_P}{\mu} \tag{2.15}$$

Here κ is the von Karman constant, E an empirical constant, U_P mean velocity at point P, κ_P the turbulence kinetic energy at point P, y_P the distance from point P to the wall and μ the dynamic viscosity.

The logarithmic law is said to be valid for $30 < y_* < 300$. In Fluent it is employed when $y_* > 11.225$. When $y_* < 11.225$ at the cells next to the wall it applies the laminar stress-strain relationship: $U^* = y^*$.

For resolving the energy component of the flow, the Reynolds' analogy for momentum and energy transport shows also a logarithmic law for the temperature. In Fluent, the law of the wall for temperature is setup out of 2 laws: 1) a linear law the thermal conduction sublayer and 2) a log-law for the turbulent region for predicting the turbulence conductance.

The difference between the momentum and thermal boundary layer is shown with the Prandtl number.

$$Pr = \frac{\nu}{\alpha} = \frac{\mu C_p}{k} \tag{2.16}$$

Where, α is the thermal diffusivity and C_p is the specific heat of the fluid.

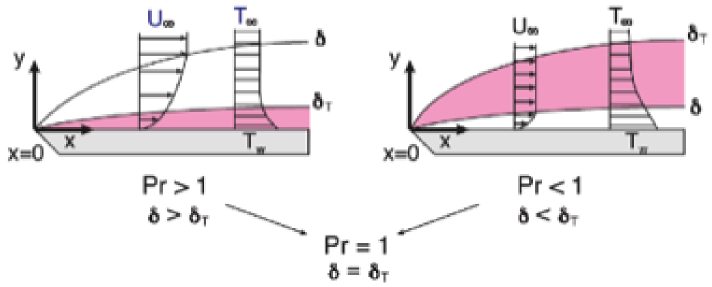

Figure 2.5: Velocity boundary layer versus the Thermal boundary layer

In Fluent the thermal law of the wall is implemented as follows:

$$T^* = \frac{(T_w - T_P)\rho c_p C_\mu^{1/4} k_P^{1/2}}{\dot{q}} \tag{2.17}$$

For $y^* < y_T^*$

$$T^* = P_R y^* + \frac{1}{2}\rho P_r \frac{C_\mu^{1/4} k_P^{1/2}}{\dot{q}} U_P^2 \tag{2.18}$$

For $y^* > y_T^*$

$$T^* = P_{r,t}\left[\frac{1}{\kappa} ln(Ey^*) + P\right] + \frac{1}{2}\rho P_r \frac{C_\mu^{1/4} k_P^{1/2}}{\dot{q}} \left\{P_{r,t} U_P^2 + (P_R - P_{r,t}) U_c^2\right\} \tag{2.19}$$

The other species dissipation are similarly tot the temperature.

Different wall functions

Modelling guidelines say that for the standard wall function, wall adjacent cells should be located within the log-law layer with a value close to the lower bound. ($y^+ \approx 30$) To prevent the cells near the wall to be in the buffer layer, the mesh should be fine or coarse enough to not have $y^+ = 5 -> 30$.

The Scalable wall functions will counteract the deterioration of the standard wall functions below $y^* < 11$. It will force the usage of the log law together with the standard wall functions. This is done with a limiter in the y^* calculation. When wall functions are preferred, the scalable wall function is recommended.

For enhanced wall treatment, when intended to resolve the laminar sublayer, y^+ should be in the order of 1. A higher y^+ is allowed as long it is well inside the viscous sublayer $y^+ < 5$. Further, the mesh should have at least 10 cells inside the viscosity affected region. This to correctly resolve the mean velocities and turbulent quantities.

In the $k-\omega$ standard model, the guidelines for wall functions should be followed. For the $k-\omega$ SST model, the enhanced wall treatment guidelines are to be followed.

In summary:

Near Wall Treatment	y^+	
Standard WF	≈ 30	minimum $y^+ = 11.25$
Scalable WF	< 30	When wall functions are used, this is the preferred option
Enhanced NWT	≈ 1	y^+ well below 5 and at least 10 cells inside viscosity affected region
All k-omega and SST turbulence models	≈ 1	same as Enhanced NWT

2.2.5 Heat transfer at Near-wall region

When the boundary layer is resolved with a laminar-sublayer, the heat flux to the wall is computed as:

$$q = k_f \left(\frac{\partial T}{\partial n}\right)_{wall} \tag{2.20}$$

Where n is the local coordinate normal to the wall.

When the flow is turbulent, the above relation 2.19 is used for finding the fluid temperature.

The wall temperature then is found from the following relation:

$$T_w = \frac{q - q_{rad}}{h_f} + T_f \tag{2.21}$$

Where q_{rad} is the radiative heat flux, which can be neglected in this case. For modelling the convective heat properties of a "bottle with a fluid inside", fluent gives the option to define an external heat transfer coefficient and external heat-sink temperature. 2.21 then becomes:

$$q = h_{ext}(T_{ext} - T_f) \tag{2.22}$$

In case of the bottles for shrink sleeving. h_{ext} where defined between 10 and 100, which is representative for natural convection of respectively air and water. T_{ext} was set at 293.15K. These were set as assumptions to have a similar thermal impact as a bottle filled with standing still air or water at room temperature.

2.2.6 Nusselt prediction by RANS-models

The 3 most often used models in literature concerning impinging jets are $k-\epsilon$, $k-\omega$ and v^2-f models.

From Fluent (2009) the $k-\epsilon$ RNG and Realizable models are explained to be improvements on the standard $k-\epsilon$ model. The RNG model has an extra term in its ϵ equation that improves the accuracy for rapidly strained flows, it has better accuracy for swirling flows and provides an analytical formula for turbulent Prandtl numbers constant values. The Realizable model further contains an alternative formulation for the turbulent viscosity and has a modified transport equation for ϵ.

The $k-\omega$ model and especially its Shear-Stress Transport variant are explained to be more robust and accurate then the $k-\epsilon$. They combine the $k-\omega$ formulation in the near-wall region and the $k-\epsilon$ model in the far field. It therefore is more accurate and reliable for a wider class of flows.

In references Sundén (2001) Heck et al. (2001) Thielen et al. (2003) comparisons are made with the commonly used 2-equation turbulence models $k-\epsilon$, $k-\omega$ and v^2-f models. The main parameters to be compared are the flow field and Nusselt number. The flow field comparison is based on the velocity profiled and turbulent kinetic energy.

In Sundén (2001) a single unconfined impinging round air jet with $Pr = 0.7$ and $Re = 23000$ to $Re = 70000$ is simulated and compared with experimental data from Craft et al. (1993).

A comparison is made between the $k-\epsilon$, $k-\omega$ and both of these models adjusted with a Realizability constraint. Fig 2.6 shows the Nusselt number and fig. 2.7 gives an indication of the turbulent kinetic energy. Both models have results that are far away from the experimental date. When the Realizable functions are used, they help with predicting the turbulence near the wall and with the Nusselt number near the stagnation point., which brings the results close the experiment data.

In Heck et al. (2001) an example is show of a Heat Transfer simulation of the cooling of a cylinder by 96 nozzles blowing at a distance of $h/d = 4$ with a Reynolds number of 17000. The flow is simulated with the Renormalization Group Model (RNG) in combination with the $k-\epsilon$ model. The RNG model will make approximations for the viscous sublayer in vicinity of the wall. This way the viscous sublayer does not need to be resolved in a grid system, which makes the numerical model robust and it safes grid points.

The paper concludes that the $RNG-k-\epsilon$ are a valid tool to investigate the flow field and

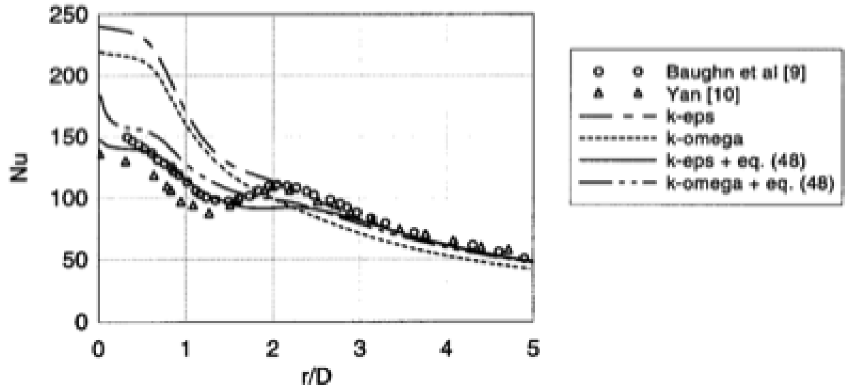

Figure 2.6: Comparison of Nusselt number for: $k-\epsilon$ vs $k-\omega$ vs $k-\epsilon$-realizable vs $k-\omega$-realizable vs experimental data

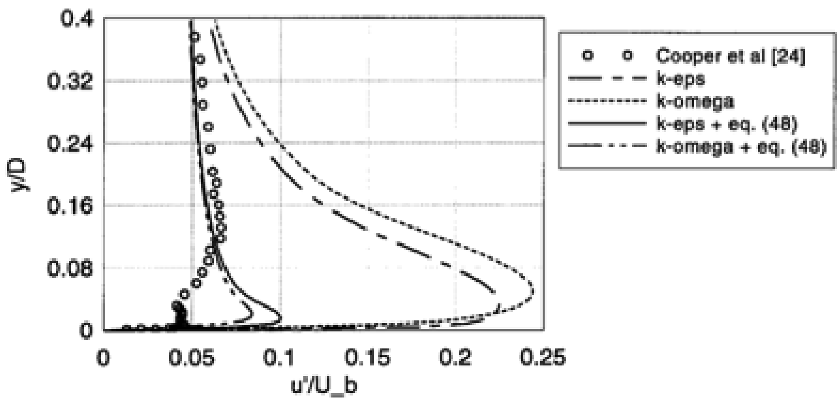

Figure 2.7: Comparison of $k-\epsilon$ vs $k-\omega$ vs $k-\epsilon$-realizable vs $k-\omega$-realizable vs experimental data

heat transfer calculations for their simulation. Since the Reynolds numbers and purpose of this paper is close to the SSL case, this is a good indication that the $RNG-k-\epsilon$ can be useful.

In Thielen et al. (2003), the $k-\epsilon$ and v^2-f models are used to for a multiple jets flow and impinging heat transfer research. The simulation is setup with 9 nozzles, the impingement wall is 4 nozzle diameters away from the nozzle outlet and a Reynolds number of 20000.

Figures 2.8 the velocity contours perpendicular to the wall are given for both the $k-\epsilon$ and $v^2 f$

model. Result are very comparable. Fig. 2.9 shows the same comparison for the turbulent kinetic energy. A distinct difference in turbulence is predicted by both models. Which will have a big influence on the heat transfer, as also seen in fig. 2.10.

The paper concludes that the qualitative overall prediction of the flow field is similar for both models. For the kinetic energy and the Nusselt prediction, similar to other references, are different in peak height and in position. The v^2-f has a more accurate prediction, which is therefore the preferred model.

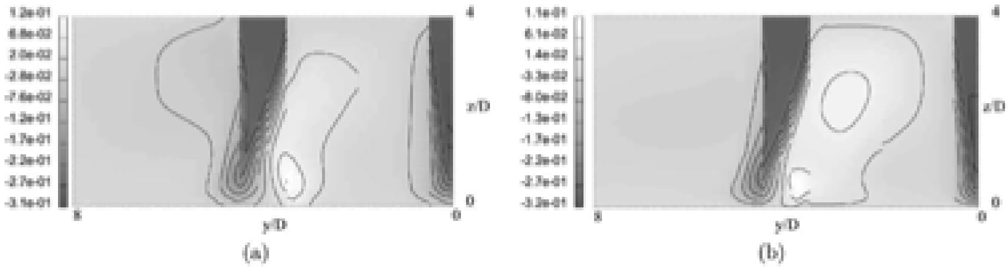

Figure 2.8: Comparison of Wall normal velocity: $k-\epsilon$ vs v^2f

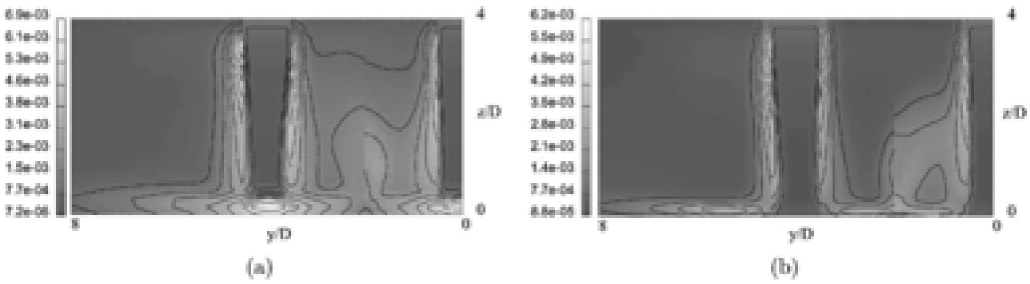

Figure 2.9: Comparison of turbulent kinetic energy: $k-\epsilon$ vs v^2f

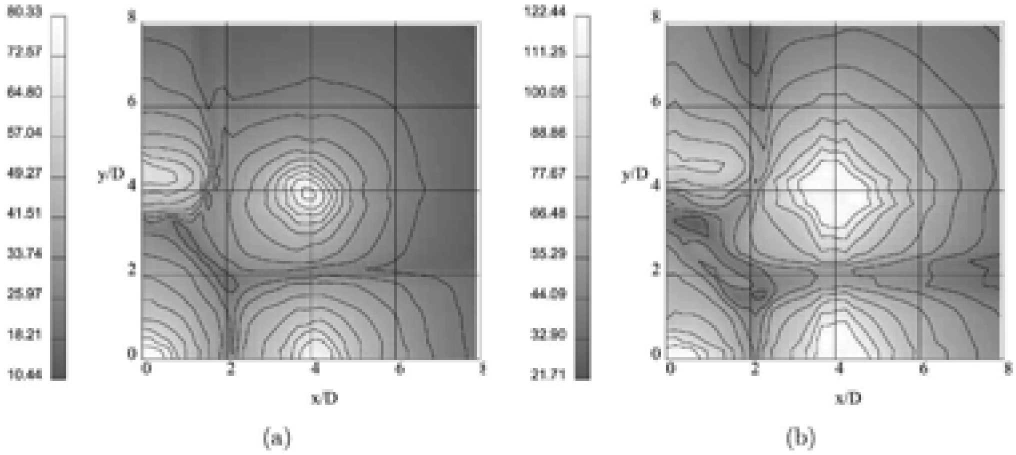

Figure 2.10: Comparison of Nusselt number: $k-\epsilon$ vs v^2f

2.3 Conclusion

From the theory a couple of concluding remarks can be made: to correctly model the heat transfer on an impinging wall, it is important to accurately resolve the flow's velocity profile and turbulence at the wall and also the temperature of the flow near the wall. The flow near the wall is mainly influenced by the nozzle jet flow and the turbulence created by the jet. The temperature of the flow is also a result of the diffusivity of the fluid in the jet flow. Once the jet flow impinges on the wall, it is important to correctly resolve the boundary layer such that the convective and conductive heat transfer to is accurately simulated.

The method to accurately resolve the nozzle jet flow will be dominated by the choice of turbulence model and by the setup of the mesh in the locations in the jet flow where high gradients are present. They will influence the accuracy of the velocity profiles and turbulent energy in the flow. The accuracy of the flow near the wall will be dominated by the wall function or near wall treatment of the flow.

From literature on turbulence models we can read that RANS-models are often used models in industry applications because of there relatively good accuracy and excel because they are time efficient. The $k-\epsilon$ $k-\omega$ and v^2f have good reference when used in jet impingement heat transfer simulations. In upcoming research we need to find out whether Realizable functions can help to enhance the stagnation turbulence prediction. Further, the RNG-function can help to reduce the grid density near the wall, which can reduce computation time. Finally, the v^2-f model seems to be a good model for the SSL-case. Since Fluent does not provide this model in its normal licenses, we probably will start our research with the $k-\epsilon$ and $k-\omega$ models.

For wall functions, the decision needs to be made based on which turbulence model will be used and based on how fine the mesh can be near the wall. When there is a restriction on mesh size near the wall, wall functions will be preferred. When a fine boundary layer mesh can be setup, the enhanced wall treatment is preferred since it fully resolves the boundary layer during the simulation. More on this follows in the next section where the turbulence models and wall functions are tested in a small impinging jet simulation.

Chapter 3

Jet impingement model

In this chapter the different steps taken to model the impingement flow are described. The first section will explain the steps taken to choose a suitable turbulence model and wall functions. Here the assumptions made and their possible errors will be shown. For the jet flow and impingement region, the grid density check will be explained, together with the upscaling of the model. In the first steps only 1 jet flow and it's impingement on a wall will be used. Later the flow of 1 full nozzle will be modelled with its impingement on a wall and later the full model with 20 nozzles and steam extraction system will be simulated.

3.1 Jet flow

To find out which turbulence model and which type of wall functions will fit for this model, a small scale model is setup. It represents 1 nozzle with diameter D, a pressure header in front of the nozzle and a wall at 10D from the nozzle exit. In this case, $D = 10mm$ is chosen based on example steam nozzles seen in literature. The specific case in this section is chosen since it represents settings in the range of the operating conditions of the steam tunnel.

The main interest of this model lies in the heat transfer capabilities from the flow to the wall, therefore the goal is to compare data of Nusselt number on the impinging wall between the simulated data and data from formerly mentioned papers. Since the flow along the wall and the impact of the flow on the wall will have an effect on the heat transfer characteristics, first the upstream jet flow and the wall flow at the impinging wall will be verified. Main characteristics for the jet flow are the velocity on the centre line of the nozzle, the velocity profiles at different sections and the turbulence intensity. For the wall flow, the incoming velocity profiles and the boundary layer velocities have typical shapes. Data for these characteristics are found in Boguslawski and Popiel (1979) and Abramovich and Schindel.

From theory section was decided to investigate the $k - \epsilon$, $k - \omega$, the SST model and their different versions.

3.1.1 Small scale setup

To focus on the turbulence models, the boundary conditions of this first model are fixed. They are defined from observation of the process at this stage, because the experiments were performed on a later date. The geometry of the model is a 3D cylindrical shaped model. The figure presented below are all side views or section views of the cylinder.

Inlet gauge pressure	200	[Pa]
Outlet gauge pressure	0	[Pa]
Inlet Temperature	370	[K]
Fluid material properties	Air	[-]
Impinging wall k	20	[-] based on free convection of air
impinging wall thickness	0.0005	[mm] Based on PET bottle thickness
Impinging wall material properties	PET	[-]
Nozzle wall material properties	Adiabatic wall	[-]

The mesh is defined in such a way it will not have an influence on the results. The assumption made is that the RANS models will average the smallest length scales of the turbulent jet flow, which lays in the order of 0.1mm according the Kolmogorov micro scales. The grid regions where the highest Turbulence Intensity are expected are meshed with these grid size as a reference. See pictures of the mesh below 3.1, 3.2, 3.3 and 3.4.

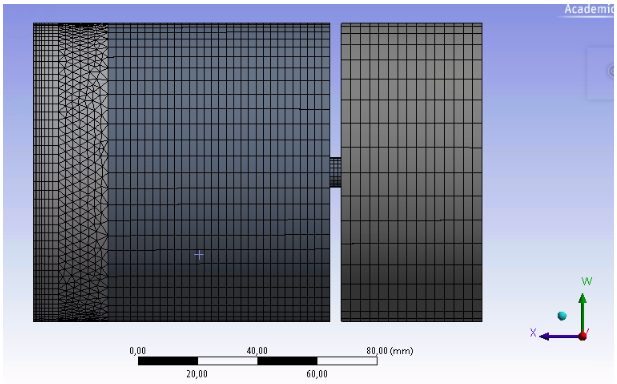

Figure 3.1: geometry

3.1.2 Turbulence model

To make a relevant comparison of the turbulence models, the velocity contours and turbulence intensity contours are shown in the following graphs as a first overview. From PIV experiments

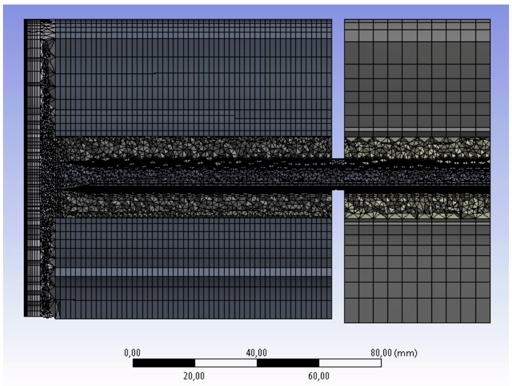

Figure 3.2: Mesh of small model: fine grid

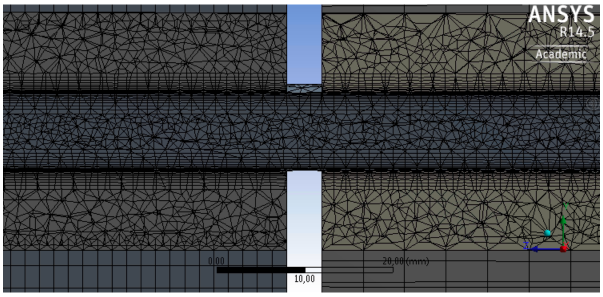

Figure 3.3: Mesh of small model: fine grid at nozzle inlet and exit

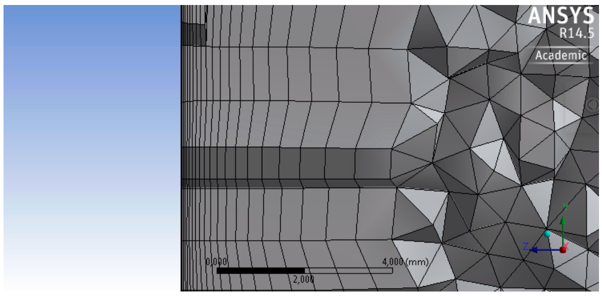

Figure 3.4: Mesh of small model: Wall inflation

in Xu et al. (2013), the velocity and turbulence intensity profiles are measured for a free jet from a circular nozzle with Re = 50000, see graph 3.5. Typical turbulent jet flows show a jet core, with an approximated length of 4 to 5 times the jet diameter. This can be seen in the left graph of 3.5, where U/U_∞ reaches $x/D = 4$. Further, the turbulence intensity of the jet is highest downstream of the jet orifice walls and dissipates after approximately 5 diameter lengths. See the left graph of 3.5.

The simulation of the jet, in our case with a wall at $z/D = 10$ but with similar inlet conditions for the nozzle, gives the results shown in velocity contour plots of the cross-section of the jet flow.

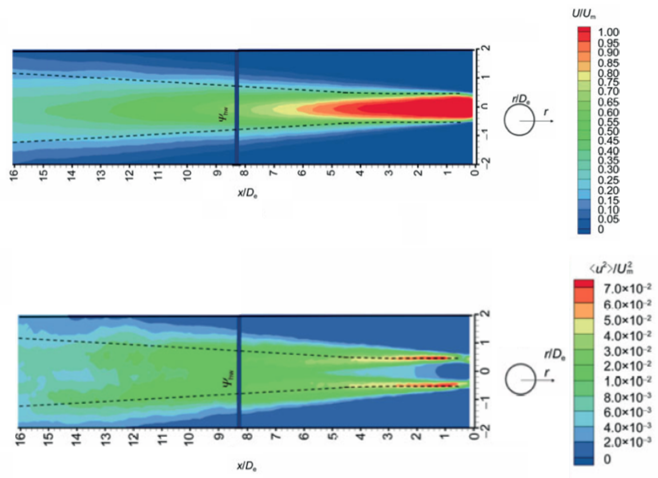

Figure 3.5: PIV normalized velocity contour from paper Xu et al. (2013)

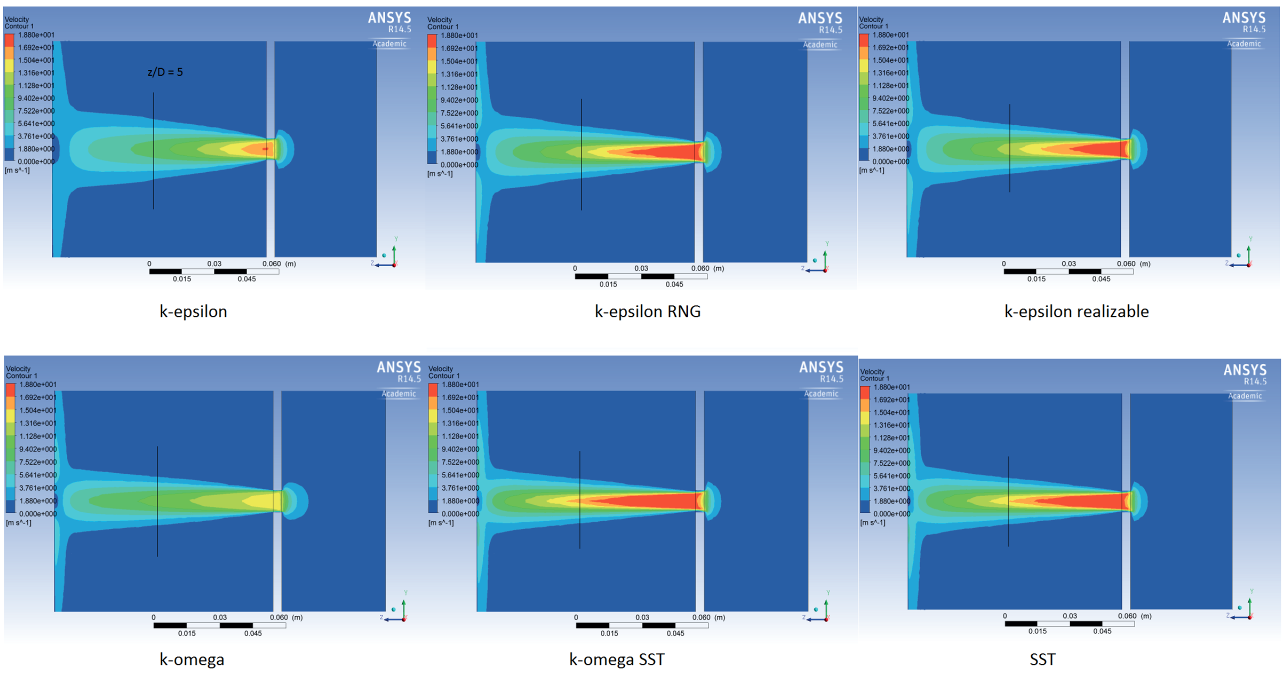

Figure 3.6: Single jet: Velocity Contours

Making a qualitatively analysis of these graphs, we can say that all models give a reasonable good velocity contour of the jet flow. Looking at the jet core length, the $k-\epsilon$ and $k-\omega$ model both have a very short jet core length of around $z/D = 3$. The $k-\epsilon$ realisable model has a jet core length of $z/D = 5$. And finally the $k-\omega$-SST and SST model have nice estimations of the jet core of approximatly $z/D = 7$. Further looking at the turbulence intensity (TI) contours, the $k-\epsilon$ and $k-\omega$ models both have an incorrect TI estimation in jet opening. The the $k-\epsilon$ realisable model shows a good TI estimation near the jet orifice walls. And the $k-\omega$-SST and SST model seem to give the best estimate of the TI. It shows a zero turbulence intensity inside the jet, which grows from the orifice walls.

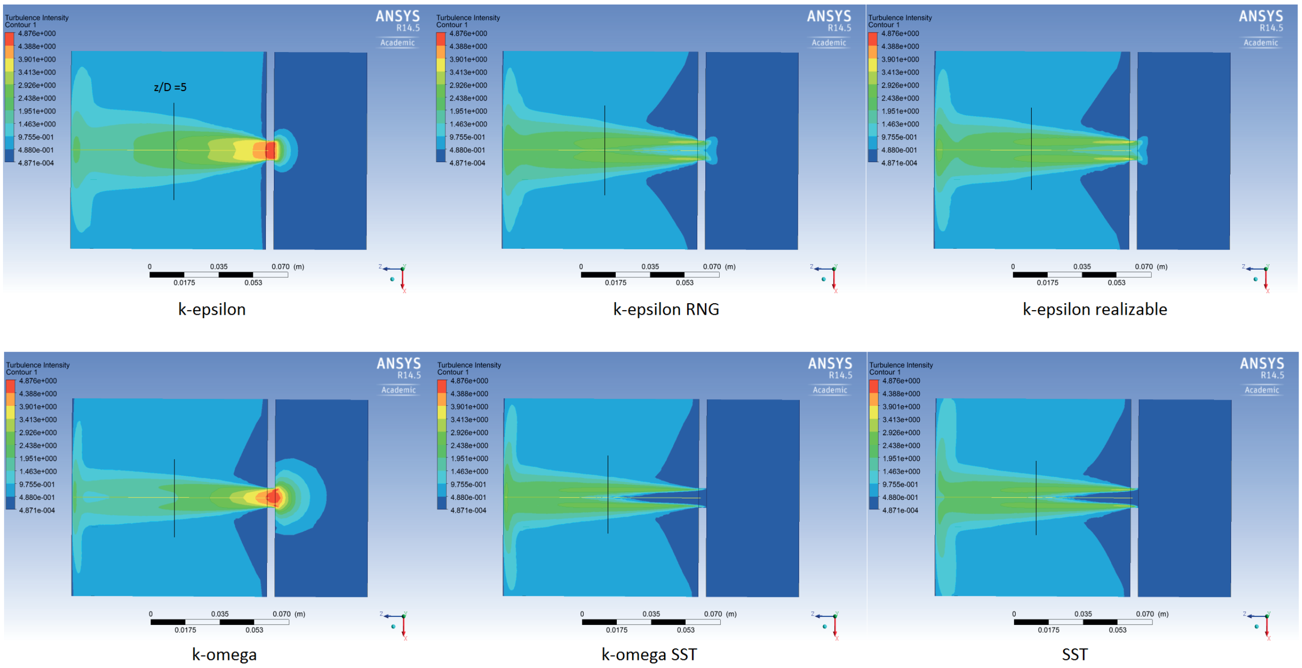

Figure 3.7: Single jet: Turbulence Intensity contours

To make these qualitative analysis more quantitive, the same CFD simulations are compared with jet measurement data from Abramovich and Schindel. Here a generalised velocity and turbulence intensity data analysis is done of the jet flow. The data shows both the velocity and the turbulence intensity on the centre axis of the flow. The velocity is normalised with the mean velocity. See graphs 3.8.

From fluent the jet flow data for all the above mentioned turbulence models are extracted and are normalised and plotted with Matlab, see graphs 3.14 and 3.15. The axis are set similar to the graph in fig. 3.8 Because the model that is used has a wall on $z/D = 10$, the velocity profiles are going steep to zero at around $z/D = 9$ The data from literature is a fully free jet. Therefore the comparison should be made in region from $z/D = 0$ to $z/D = 9$

When comparing these velocity and turbulence intensity data with the simulations, the $k-\omega$ SST, and SST models are found to be better in predicting the flow velocity profiles behind the nozzle. Also the $k-\epsilon$ realisable model gives a good velocity prediction, but has a small deviation on the TI results. The standard $k-\epsilon$ and standard $k-\omega$ models are the worst, especially in predicting the turbulence intensity.

Next, to check the ability of the turbulence models to predict the temperature inside the flow, normalised temperature profiles are compared with data coming from Abramovich and Schindel, see graph 3.11. The profiles are showing the flow at a distance of $z/D = 2$, downstream of the nozzle. The data used are experimental data from hot air experiments, normalised for the mean velocity and mean temperature of the jet flow. Within the jet core, up to maximum $z/D = 5$ these graphs are generic.

Structure of the free round turbulent jet 535

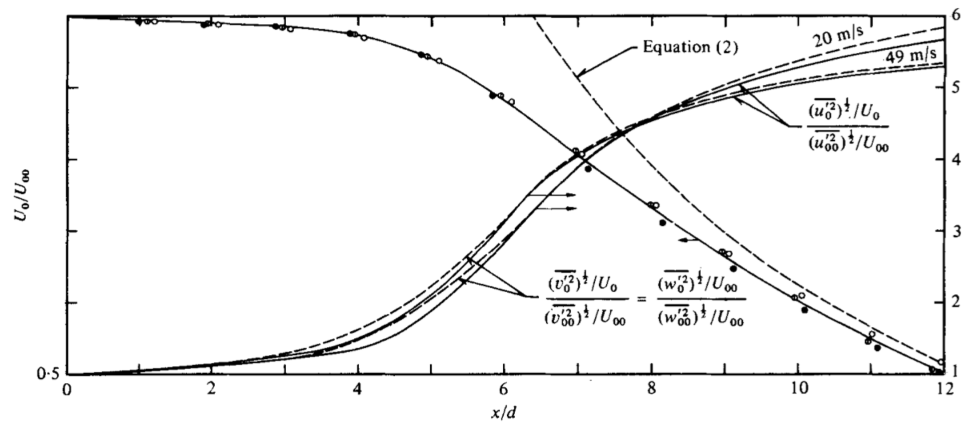

Figure 6. Axial variation of the longitudinal mean velocity and relative turbulent intensities on the jet centre-line. ○, $U_{00} = 20$ m/s; ⦶, $U_{00} = 30$ m/s; ●, $U_{00} = 49$ m/s. $(\overline{u'^2})^{\frac{1}{2}}/U_{00} = 3{\cdot}8 \pm 0{\cdot}1$ %,

Figure 3.8: Axial mean velocity and turbulent intensities of jet centre line

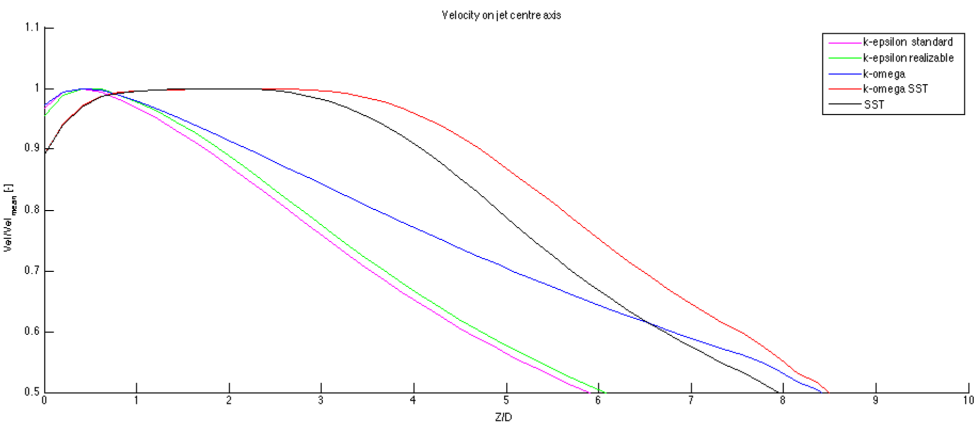

Figure 3.9: Non-dimensional Velocity on center axis: k-epsilon, k-epsilon enhanced, k-omega, k-omega SST, SST

Here we can see that there are no big differences of the models to predict the temperature profiles. Therefore, when there is a good result for the velocity profiles, the energy equation will be able to accurately predict the temperatures.

Conclusion turbulence models

From these results a first selection of turbulence models is made. The $k-\epsilon$ realisable ,$k-\omega$ SST, and SST models where clearly better in predicting the velocity, turbulence intensity. In the upcoming section, they will only be taken into account.

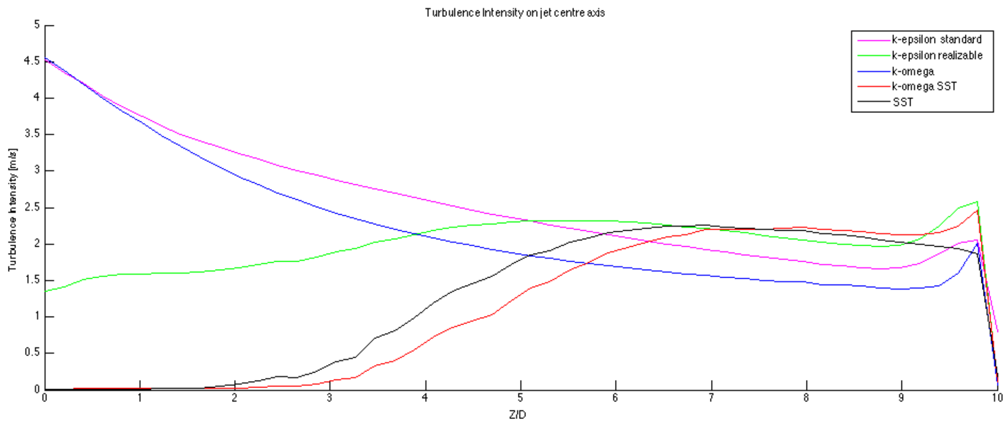

Figure 3.10: Turbulence Intensity on center axis: k-epsilon, k-epsilon enhanced, k-omega, k-omega SST, SST

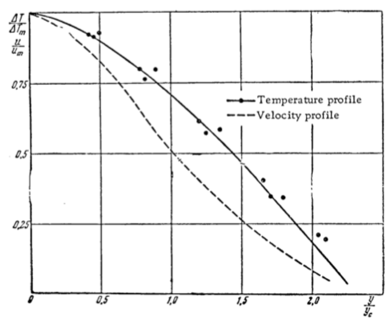

Figure 3.11: Normzalised temperature profile

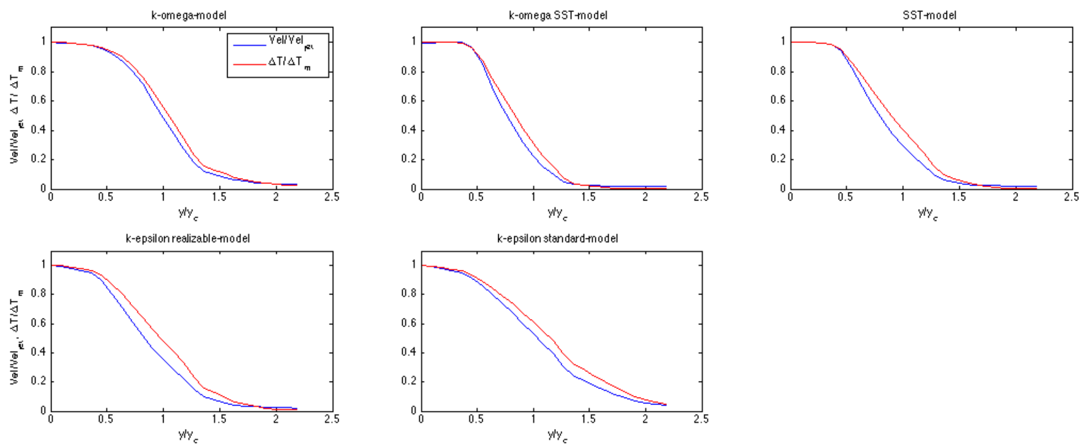

Figure 3.12: Velocity and Temp profile for z/D = 2: k-epsilon, k-epsilon enhanced, k-omega, k-omega SST, SST

Coarse mesh

Currently the mesh is very fine to make sure it does not interact with the results coming from the different turbulence models. In a next step the mesh density will be changed to a much coarser mesh, and the results will be compared with the former results.

The current mesh, see 3.2 has a total cell amount of 800.000. A next model of 130.000 cells is setup, see 3.13. This mesh coarseness is mainly found by trial and error. In case the mesh was too coarse, convergence in Fluent was not possible.

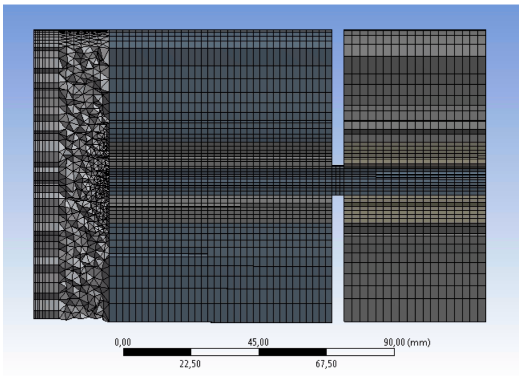

Figure 3.13: Mesh of small model: fine grid

To find out whether this coarse mesh has similar results as the fine mesh, the same plots as before are made. The velocity and turbulence intensity over the nozzle centre-line, and the velocity and temperature profiles at $z/D = 2$.

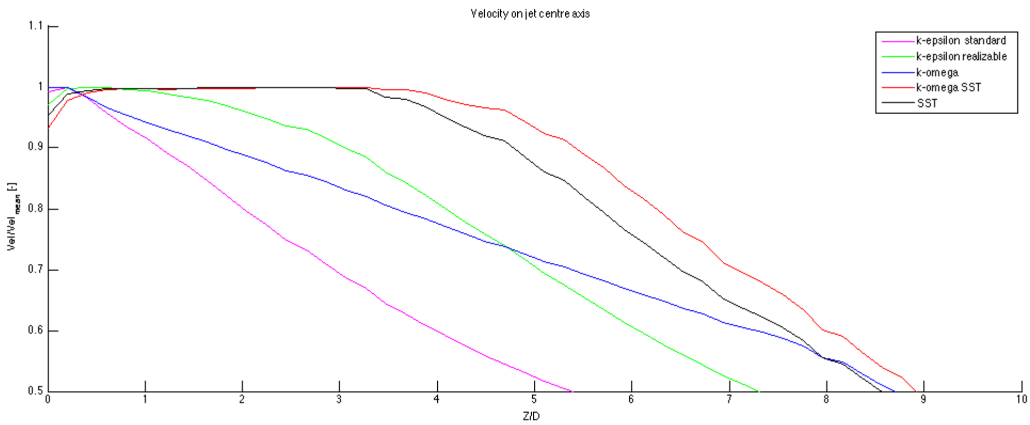

Figure 3.14: Non-dimensional Velocity on center axis: k-epsilon, k-epsilon enhanced, k-omega, k-omega SST, SST

From this can be concluded that the jet flow and temperature profiles are solved correctly with consistently with both mesh sizes. According the temperature profiles from 3.12 and 3.16, there is no big difference in the ability of the models to solve the temperature profiles.

The coarsening of the mesh did not have an influence on the $k - \omega$ SST and SST model. It did show a slight shift of the velocity profile for the $k - \epsilon$ realisable model. Still, this model seems to be enough accurate to check in the next sections for its performance on modelling a wall flow.

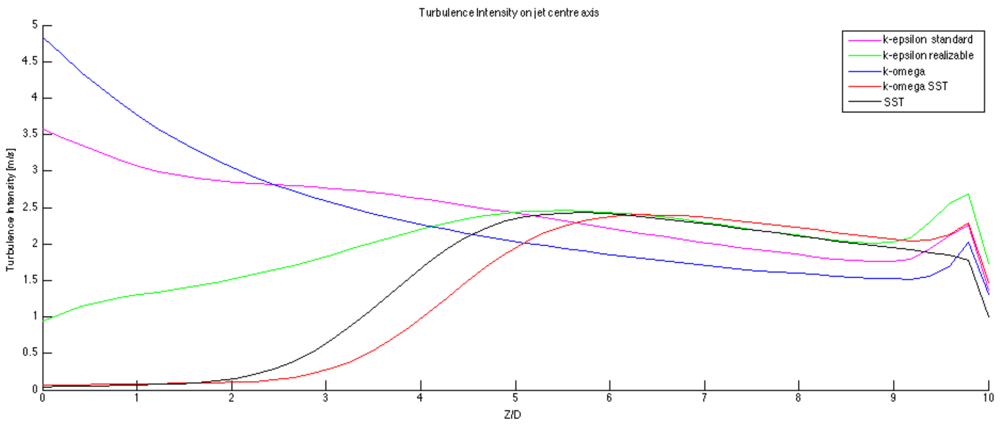

Figure 3.15: Turbulence Intensity on center axis: k-epsilon, k-epsilon enhanced, k-omega, k-omega SST, SST

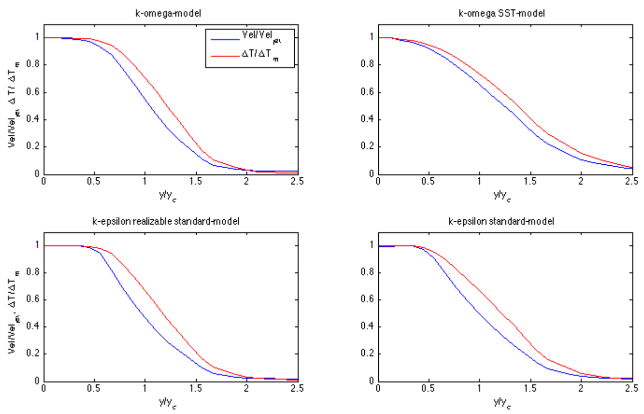

Figure 3.16: Velocity and Temp profile for z/D = 2: k-epsilon, k-epsilon enhanced, k-omega, k-omega SST, SST

3.2 Wall flow

In the next section, the focus will be on the wall flow. The flow involves a stagnation region and a wall jet. In the former chapter, we could see the advantages and disadvantages of the different turbulence models. Since we are interested in the interaction between the flow and the wall, the so called near-wall effects become important. In section 2.2 the differences in near-wall treatments and wall functions is explained. For the $k-\epsilon$ models the choice can be made between the standard wall function, the scalable wall function or the enhanced wall treatment. The $k-\omega$ SST and SST model, only gives the possibility to use enhanced wall treatment.

3.2.1 Wall functions

To compare the wall functions, a set of simulation is done with different inflation meshing on the impinging wall. The inflation is setup such that the y^+ values are approximately 1 at the impinging wall. Since the flow velocity profiles are not all the same for the different turbulence models, the y^+ can not exactly defined. Therefore a range is determined, wherefore different mesh sizes are simulated. From the theory section is shown that the near wall treatments and wall functions have certain meshing criteria, see below.

Near Wall Treatment	y^+	
Standard WF	≈ 30	minimum $y^+ = 11.25$
Scalable WF	< 30	When wall functions are used, this is the preferred option
Enhanced NWT	≈ 1	y^+ well below 5 and at least 10 cells inside viscosity affected region
All k-omega and SST turbulence models	≈ 1	same as Enhanced NWT

From figures 3.6 the highest velocities at the wall are estimated to vary between $3m/s$ and $6m/s$. The shear stress on the wall are maximum 1 Pa, the kinematic viscosity for air at 70 deg C is $20.76e^{-6}m^2/s$, density is 1,05 kg/m^3. For y^+ to be approximately 1, the smallest cell height should be between $y = 0.1mm$ and $y = 0.05$ mm. As said in the theory, especially for the less advanced standard wall function, it is important to know y value and setup the first layer mesh thickness accordingly.

Data for omparison of flows with similar conditions could was not found in literature. To still have a reference for the velocity profiles, the boundary layer thickness on the wall is approximated with equation 3.1, coming from Wang et al. (1989). It is a function for the wall flow of an impinging jet and is relevant outside of the stagnation zone. $z/D < 1$. It is plotted in 3.17 and then compared with the CFD results shown in figures 3.18. In the CFD results, δ is taken as the position of the maximum of the velocity plots.

$$\delta(r) = \sqrt{\frac{420}{37}\frac{\nu}{U_0}r + \frac{c}{r^2}} \tag{3.1}$$

Where,

$$c = 0.81\frac{\nu}{U_0}D^3 \tag{3.2}$$

and

$$\tau_w = 0.058/Re_x^{1/5} \tag{3.3}$$

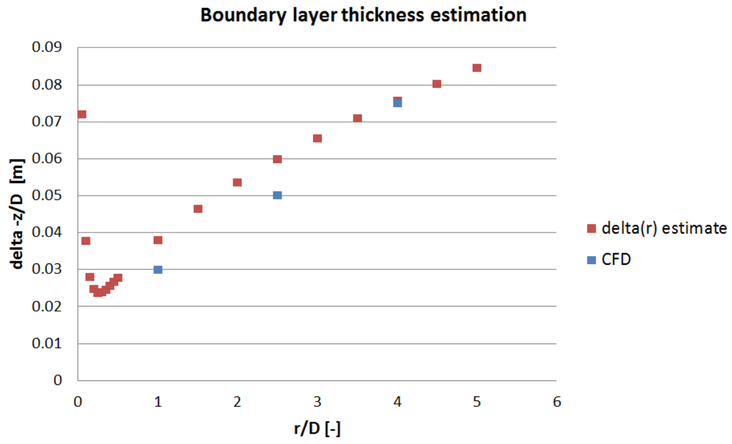

Figure 3.17: Boundary layer thickness on impingement wall

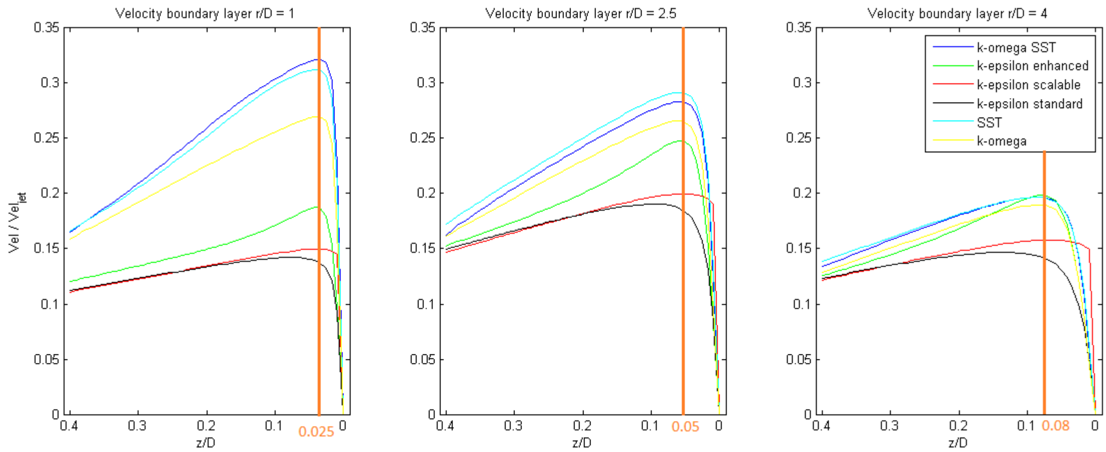

Figure 3.18: Velocity boundary layer at r/D= 1, 2.5 and 4 for mesh with $y^+ < 1$

With the CFD results from the very fine mesh, the boundary layer at the wall is plotted. This mesh has a first layer thickness of 0.03mm, so the full viscous and turbulent boundary layer should be calculated according the Law-of-the-wall for the k-omega and enhanced wall functions. From the CFD results can be seen that the scalable wall function gives an error, since it models the viscous sub layer in the cells adjacent to the wall. The results from all k-omega and SST models show a good result for the boundary layer, together with the k-epsilon enhanced results. The k-epsilon standard and scalable both seem to be in-accurate.

In a next step, the $y+$ values are set to ≈ 1 to see its effect on the near wall velocities of the jet. As mentioned before, the $y+$ values can not be estimated very exact, since Re_x can not easily be calculated. The mesh is given an inflation with first layer thickness of 0.10mm, which is based on $Re_x = 5000$ for the flow at $5m/s$ at $r/D = 2$ In graph 3.19 they are checked with the $k-\epsilon$ scalable, enhanced wall treatments and with $k-\omega$ and $k-\omega$ SST. The standard wall function is not used, since it needs a much coarser mesh, see 3.2.1.

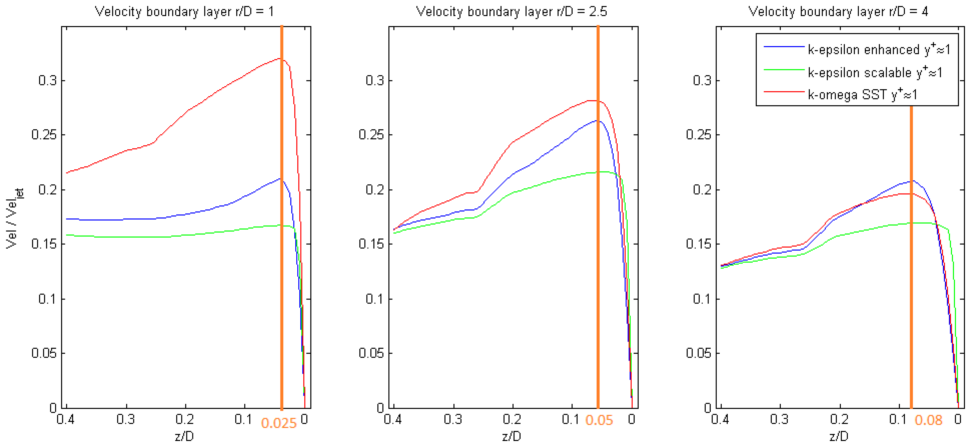

Figure 3.19: Velocity boundary layer at r/D= 1, 2.5 and 4 with $y^+ \approx 1$

From these results we can conclude that the $y+ = 1$ mesh gives very similar boundary layer velocity results then the very fine mesh. The $k - \omega$ and $k - \omega$ SST models have a larger amplitude of the velocity. The $k - \epsilon$ enhanced model shows a very similar overall shape of the boundary layer. Only the scalable wall function results in to a different boundary layer profile. Its thickness δ seams to lay around the first layer thickness of the mesh.

Coarse Mesh

To see how good the boundary layer is resolved on a much more coarse mesh, the $y+$ value is increased to 11.25, which means a first layer inflation thickness at the wall is 0,5 mm. This coarseness is chosen because it matches the recommendations from the fluent theory guide to use for scalable and standard wall functions. This mesh is tested on all the k-epsilon and k-omega models, to also see the impact on the upstream flow coming from the jet.

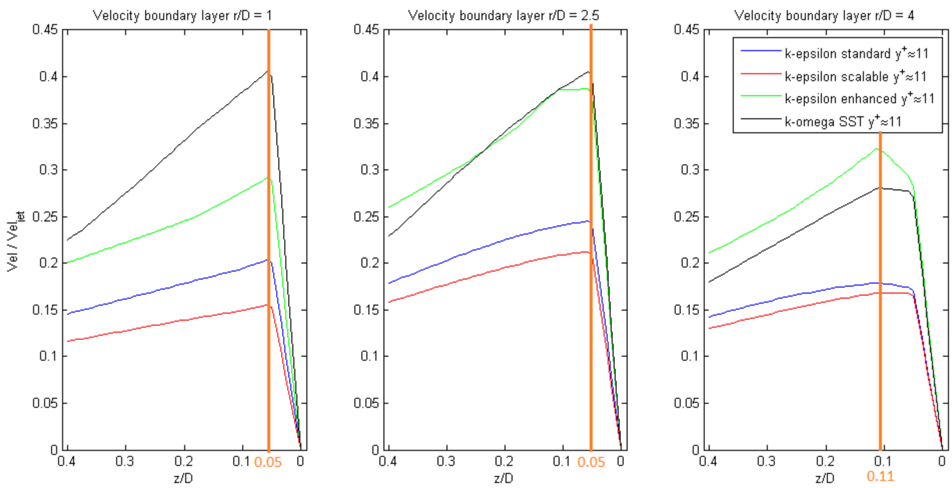

Figure 3.20: Velocity boundary layer at r/D= 1, 2.5 and 4 for coarse mesh with $y^+ \approx 11$

The results show a significant difference with the former boundary layers. All the models now resolve the first cell as a viscous-sublayer. Further upstream, the flow shows very similar behaviour as the flows calculated with the finer meshes. Since coarser models will be needed in order to be able to solve the entire geometry of the shrink sleeve tunnel, the impact of these deviations will be explained in the next section.

3.2.2 Heat transfer

To show how the turbulence models and near wall treatment effect the heat transfer results, the the Nusselt number is calculated with Matlab from the CFD data. This is done according equations 3.5. As said before, the Nusselt number is dependent on Re, z/D, r/D and Pr. In the test case $z/D = 10$, $Re_d = 7500$, and $Pr = 0.74$. So the Nusselt number is plotted according the radial distance from the jet axis, r/D.

Two important characteristics that are used to compare the data from literature and the CFD data are 1) the general shape of the graph and 2) the stagnation Nusselt number, which is the Nu at $r/D = 0$.

In Liu et al. (1991), an empirical correlation between the $Nu_{stagnation}$, Re, Pr and z/D is shown for turbulent circular jet flows, see 3.4. It is usable for flows with $4000 < Re_d < 52000$, with an average error of 15 %.

$$Nu_{stagnation} = 1.51 Re_d^{0.44} Pr^{0.4} (z/D)^{-0.11} \tag{3.4}$$

From this, we calculate that Nu_d for the test case to be 54.1, with the error margins an estimate is $45 < Nu_d < 62$.

From Jambunathan et al. (1992) and ODonovan (2005) reference values where found to compare the overall shape of the Nusselt - r/D graph. The graph shows measurement data from experiments on normal impinging air jets, where heat is measured with a hot film sensor. The Diameter of the nozzle is 10mm and distances for z/D are measured between 2 and 8 and the Reynolds number vary between 10000 and 30000. The exact data taken from the graph has $Re = 10^4$, $z/D = 8$, see figure 3.21

From the simulations in Fluent, the Nusselt number is calculated as follows:

$$Nu = \frac{h_w D}{k} \tag{3.5}$$

For which h_w is the wall heat transfer coefficient on the wall and k is the thermal conductivity of the fluid. The heat transfer coefficient is:

$$h_w = \frac{q}{\Delta T} = \frac{q}{T_w - T_{reference}} = \frac{q}{T_w - T_{jet}} \tag{3.6}$$

Here, q is the heat flux through the wall, T_w the wall temperature and T_{jet} the average jet temperature on the centreline. Since Fluent calculates the Nusselt number with a fixed reference number, this data was post-processed according to common practice found in ODonovan (2005).

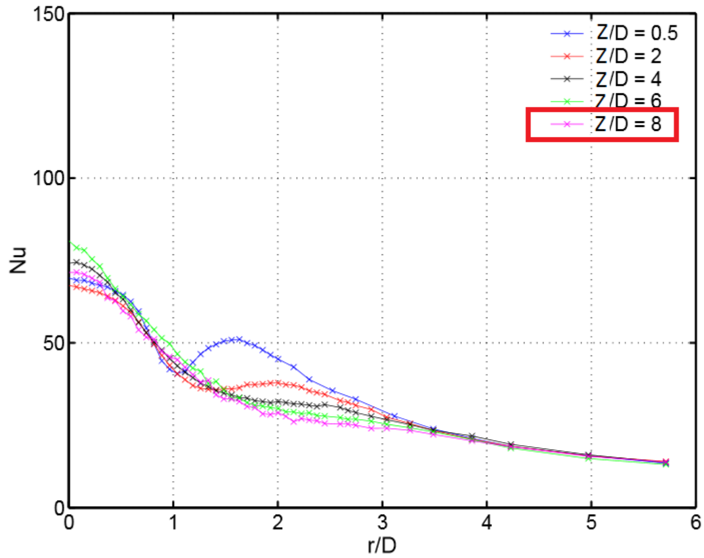

(a) $Re = 10000$

Figure 3.21: Nusselt number at impingement wall data from Jambunathan et al. (1992)

Comparing these data sets, see figures 3.21 and 3.22, the overall shape of the Nusselt number graphs for all models are accurate comparing with the data-set. They have a clear maximum at the stagnation area $0 < z/D < 1$ and go to $Nu \approx 10$ after 5D distance.

Further the Nusselt number at the stagnation point is largely over-predicted by both the $k-\epsilon$ standard WF model. The $k-\epsilon$ enhanced WT model slightly under-predicts at the stagnation point comparing to the calculated range of of $45 < Nu_d < 62$. The $k-\omega$ SST and SST model are all just above the calculated range.

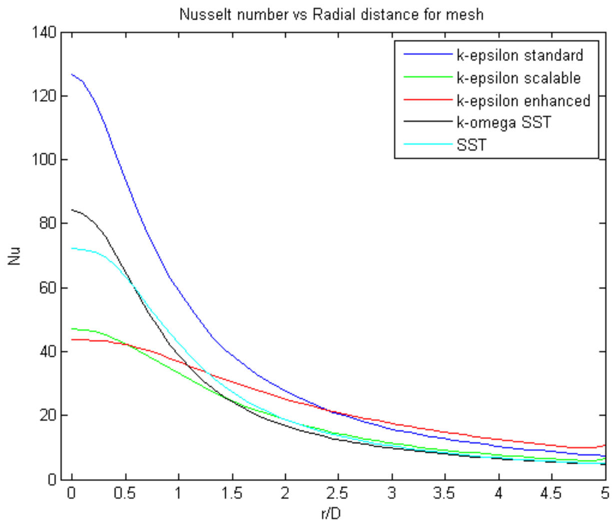

Figure 3.22: Nusselt number on impingement wall at radial distance r/D

Wall functions

To find the influence of wall functions on the prediction of the Nusselt number, it is modelled with a mesh of $y^+ \approx 1$. To show the differences, the $k-\omega$ models and $k-\epsilon$ models with wall functions, see fig. 3.23.

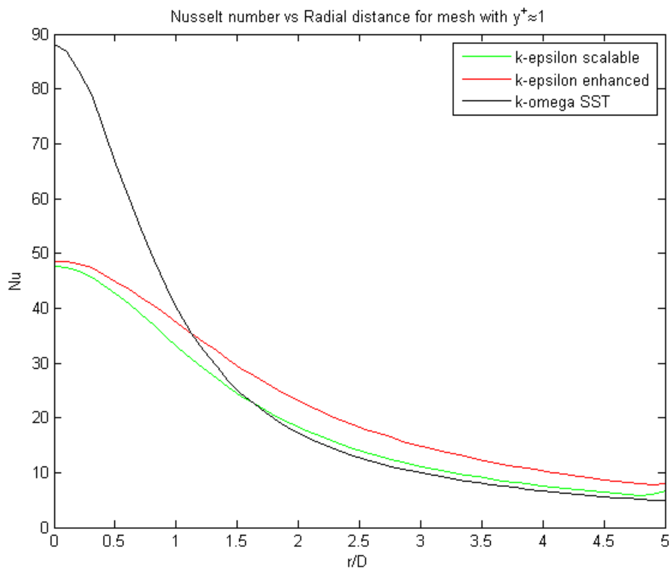

Figure 3.23: Nusselt number on impingement wall at radial distance r/D: mesh with $y^+ \approx 1$

From these results we can see that the $k-\omega$ SST model again both over predict the stagnation Nusselt number comparing to the reference value of $45 < Nu_d < 62$ calculated in (3.4). From $r/D = 1$ they gave similar results to the $k-\epsilon$models. Also the overall shape of the models are correct. Both the $k-\epsilon$models give a similar prediction of the stagnation Nusselt number as the former results.

Finally the results of the coarse mesh with $y^+ = 11$ is are plotted in the same way in fig. 3.24. Since the Standard wall function is applicable in this case, it is also plotted.

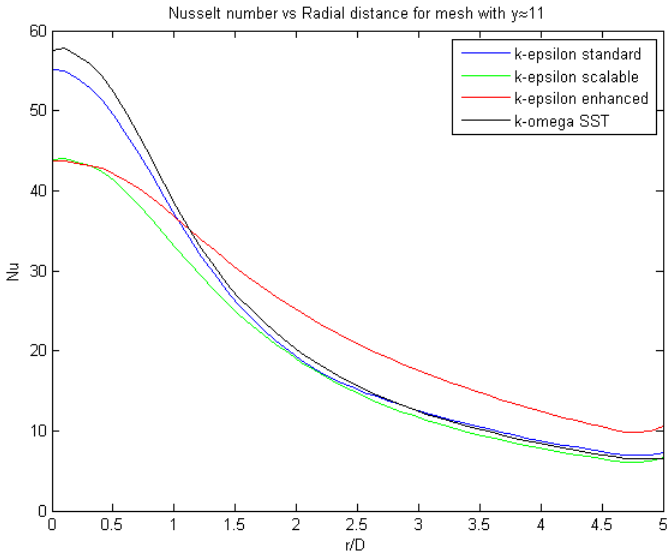

Figure 3.24: Nusselt number on impingement wall at radial distance r/D: mesh with $y^+ \approx 11$

The results here are a bit unexpected. Since the mesh is too coarse for the enhanced near wall treatment and k-omega models, they are expected to give a worse outcome. Non the less, they all give a prediction of the stagnation Nusselt within range. And also the shape of all graphs seems to be correct. A check was done with fluent data to see wether the calculated Nusselt numbers are correct. Also here their was an unexpected change in Nusselt number at the coarse mesh.

3.2.3 Conclusion

From checking the wall functions and enhanced wall treatment we can see that for y^+ sizes of 1 or less, the $k-\epsilon$ standard and $k-\omega$ SST models both over predict the stagnation Nusselt number. The $k-\epsilon$ with scalable wall function and with enhanced wall treatment both are accurate in predicting Nu_{stag}. For coarser wall inflation, $y^+ \approx 11.5$, all Nu_{stag} predictions seem to become closer to the calculated value $45 < Nu_d < 62$, in contradiction with literature and Fluent tutorials.

The $k-\epsilon$ enhanced WT, $k-\epsilon$ scalable and $k-\omega$ SST gave sustained good predictions of the Nusselt number with $y^+ \approx 1$ these will be the preferred models. For the coarse mesh with $y^+ \approx 11$ the models behave in a unpredictable way comparing to what literature tells us. Therefore the choice is made to mesh the impinging walls (the bottle in the full scale model) with a mesh thickness of ≈ 1.

Chapter 4

Nozzle & Full scale tunnel model

4.1 Nozzle model

An important part of the flow in the SSL tunnel is induced by the particular setup of the nozzle. See picture 4.1. For more details, see chapter in the Nozzle section of the background section 1.3 . A specific model is setup to find out how the different nozzles interact and where attention should be paid in the final model. Further, since all the nozzles have circular jet outlets, a simplification of the geometry is purposed to make the model easier to solve in the final full tunnel model. Since the research now is in a stage where validation via literature is not possible any more, the specific cases that are simulated in this chapter are based on available equipment. Since the research is done at P&G and in collaboration with their supplier Fuji Seal, the nozzle dimensions are roughly based on nozzles of one of their steam tunnels.

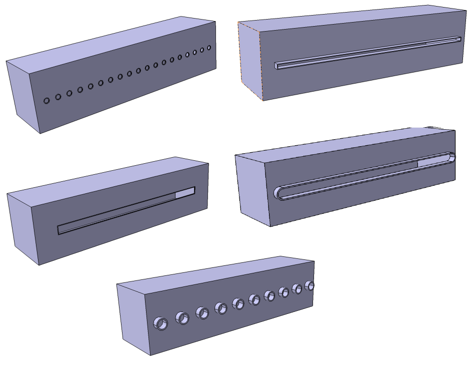

Figure 4.1: Example nozzles

For this model, the choice of the nozzle was based on the fact it has the highest flow rates and heat transfer rates. It therefore was expected to be the easiest way to show the particular effects of the nozzle interactions. The mesh of the nozzle is shown in graph 4.2 and 4.3, respectively a top section view and side section view. In 4.2 the domain in the top of the graph represent the nozzle volume and the lower domain is the opening where the nozzle flows to the impingement wall. In reality, the nozzles are supplied with steam through a flexible pipe. Inside the nozzle, an internal wall spreads the steam pressure over the nozzle's outlet holes. In this the fluent model, the pressure header is not simulated. Instead the nozzle domain is setup with a constant pressure inlet, which has a similar spreading effect as the real nozzle.

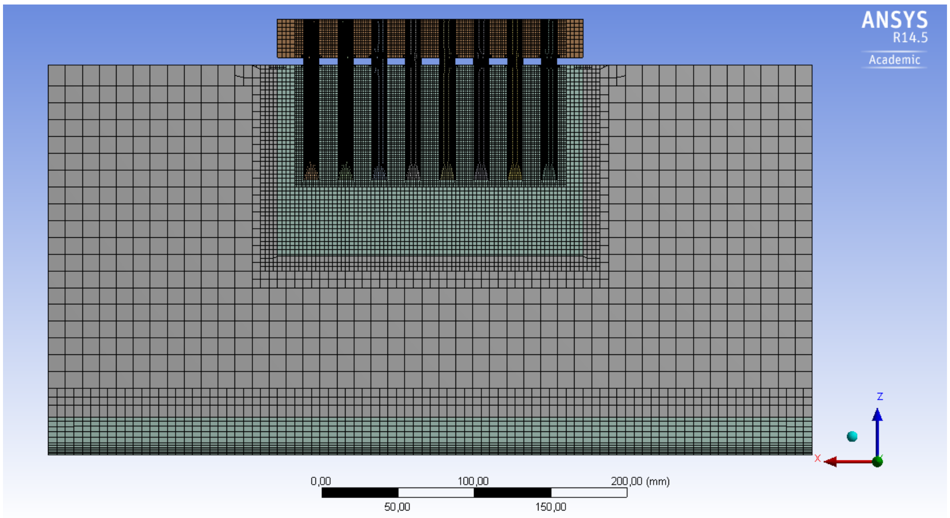

Figure 4.2: Top-view cross-section of circulare nozzle mesh

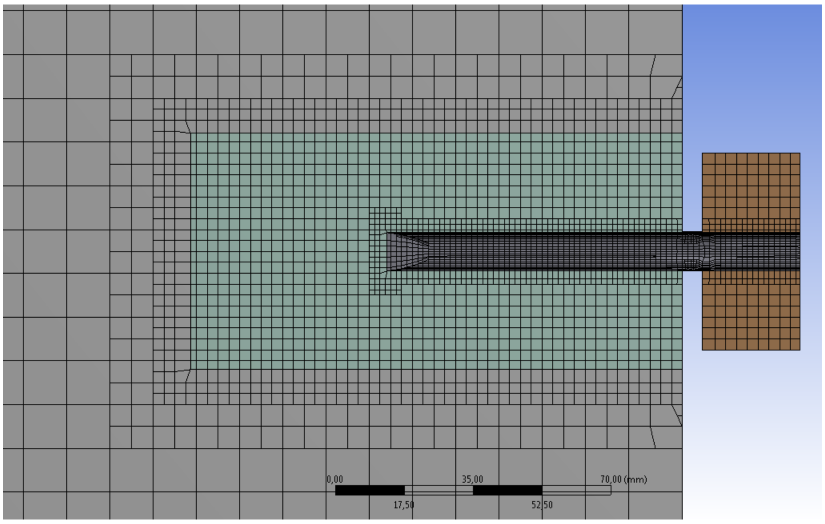

Figure 4.3: Side-view cross-section of circulare nozzle mesh

The input variables of the Fluent model are the same as the first "Jet impingement" model. They are again based on basic settings measured during testing. See chapter 5.

Inlet gauge pressure	200	[Pa]
Outlet gauge pressure	0	[Pa]
Inlet Temperature	370	[K]
Fluid material properties	Air	[-]
Impinging wall k	20	[-] based on free convection of air
impinging wall thickness	0.0005	[mm] Based on PET bottle thickness
Impinging wall material properties	PET	[-]
Nozzle wall material properties	Adiabatic wall	[-]

The mesh setup is based on the experiences from chapter 3. Since the Fluent meshing tool does not allow to copy-paste a mesh, similar settings are used with some adaptions for the specific geometry. With a new function, since ANSYS 14, in the meshing tool, a "cut cell" approach is taken in the last meshes. This provides a fully cartesian mesh instead of tetrahedral. This method was chosen because in the final model a sliding mesh will be used. To match the interfaces between the static and moving mesh, a cartesian mesh is best. The down side is, that circular shapes need a very fine mesh to give an accurate representation. Therefore, in the next section, a solution will be presented.

The turbulence models used in this model are both the $k-\epsilon$ realizable and the $k-\omega$ SST. From chapter 3, these 2 models were proven to be best. These 2 models will be used to compare results and find out which of the 2 works best.

4.1.1 Nozzle flow results

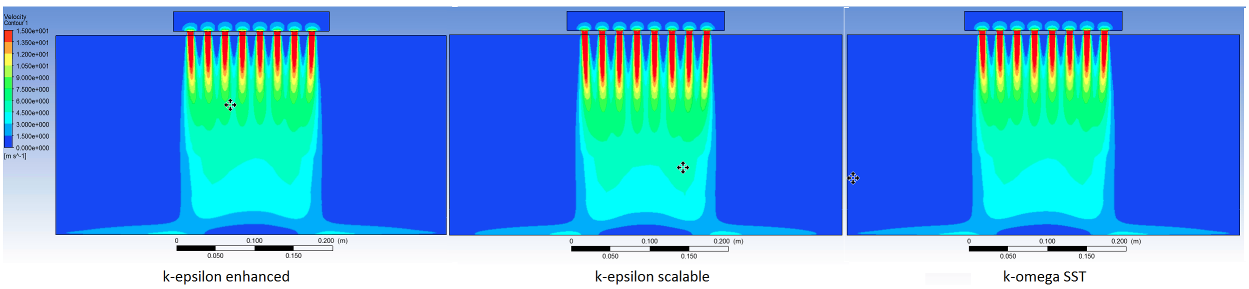

Figure 4.4: Velocity contours at Nozzle cross-section

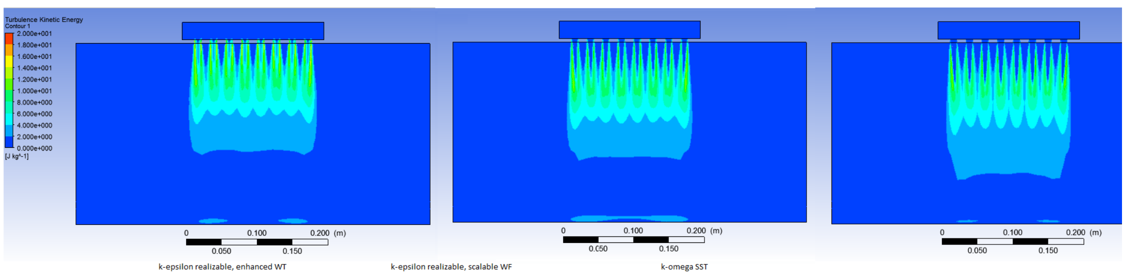

Figure 4.5: Turbulence intensity at Nozzle cross-section

As expected, the nozzle nozzle flows from these models are show no deviations from the 1-nozzle simulations done in the former chapter, see 3.6. From this point, enough confidence can be given to the correctness of the results of the flow with this mesh and turbulence models. Now the interesting part of these flows are the resulting heat flux and temperatures they convey to the wall. In the following graphs, the heat flux and temperatures are plotted on the impinging wall. In this case, the wall is positioned 25 jet diameters behind the nozzle. Which is a representable case for the real tunnel.

The heat flux is interesting because it represents the energy taken per second per square meter. In the case of shrink sleeve labelling, the impinging material will not always be the same, so the heat flux will be the driving factor behind the heating of the material. In this simulation, the material of the impinging jet represents a 50 micrometer PET flat surface. The $y+$ for this mesh is approximately 1, therefore all models should be able to represent good heat transfer characteristics.

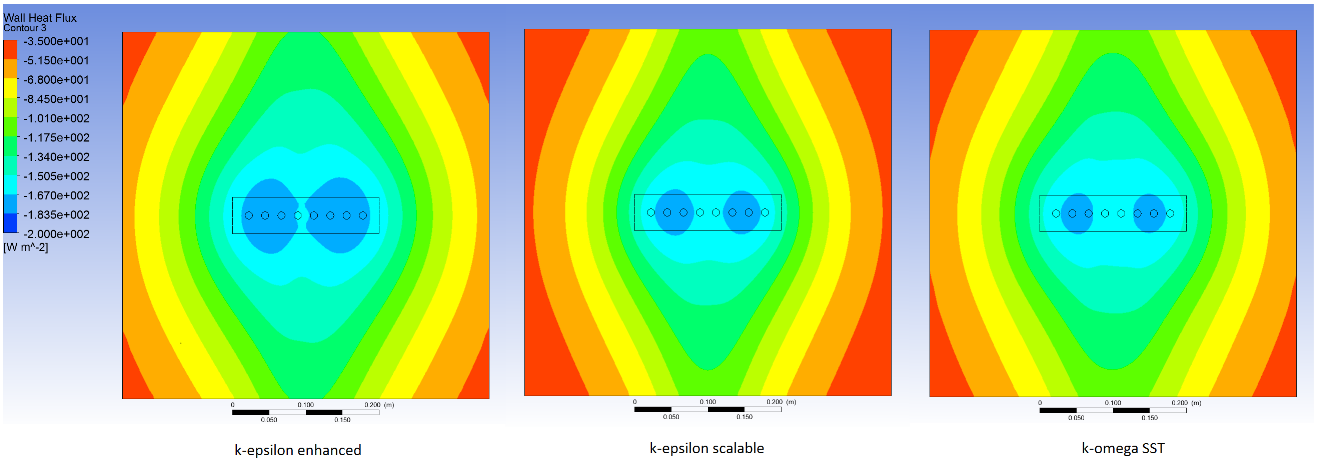

Figure 4.6: Heat flux contours on impinging wall

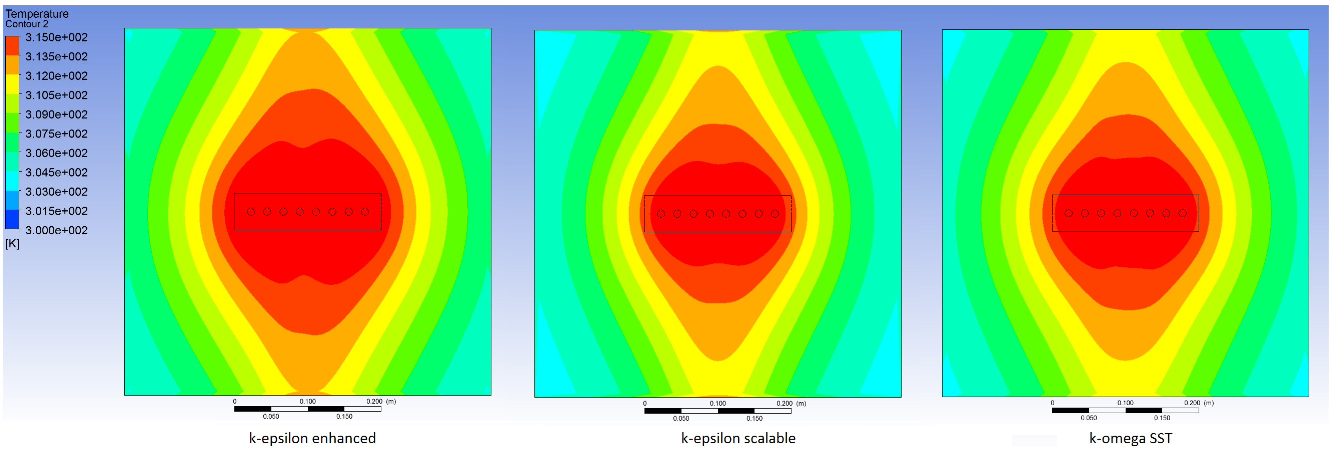

Figure 4.7: Temperature contours of impinging wall

The resulting heat flux and temperature contour's shapes are all very similar. Fig. 4.6 show

2 regions straight behind the nozzle where an increased heat flux is induced. The full region around it is the stagnation region of the flow and the 2 increased heat fluxes are induced by the a higher turbulent kinetic energy. Similarly fig. 4.7 show a higher temperature of the convective wall around the stagnation region. Since the flow is more bended upward and downward, the heat flux and temperature contours are stretched in vertical direction. The $k-\epsilon$ enhanced model shows a slightly higher heat flux and temperature, but overall all models give intuitive results.

4.1.2 Slot flow

From the velocity contours shown in graph 4.4 can be seen that, for distances of $z/D = 10$ and more, the flow starts to become similar to a "slot jet". As said before, the circular shaped nozzles are hard to mesh with a cartesian mesh, which makes the mesh less suitable for sliding mesh simulations. For this, a solution is found by modelling the circular shaped jet outlets as 1 slot.

The diameter of the jet openings are 10mm in diameter, which gives them a total area of $626mm^2$. Representing the nozzles by a $160mm$ x $3.8mm$ slot gives the flow the same width and area. Giving the geometry an all rectangular shape, it will be be able to give an accurate cartesian mesh, see graph 4.8. This results in a mesh of approximately 300.000 cells, comparing to 500.000 cells for the mesh with circular jets. With this slot nozzle and the same boundary conditions as the circular nozzle, simulations with the $k-\epsilon$ enhanced WT, $k-\epsilon$ scalable WF and $k-\omega$ SST are done for comparison. The boundary conditions are defined as:

Inlet gauge pressure	200	[Pa]
Outlet gauge pressure	0	[Pa]
Inlet Temperature	370	[K]
Fluid material properties	Air	[-]
Impinging wall k	20	[-] based on free convection of air
impinging wall thickness	0.0005	[mm] Based on PET bottle thickness
Impinging wall material properties	PET	[-]
Nozzle wall material properties	Adiabatic wall	[-]

To find out how similar the flows of the slot nozzle jet is, the same plots as for the circular jet are represented: the velocity contours, turbulence kinetic energy, wall heat fluxes and wall temperatures are shown in respectiveley graphs 4.10, 4.11, 4.12, 4.13.

The velocity contour show very similar profiles comparing the different turbulence models. Both the $k-\epsilon$ models show a stronger stagnation region, which is the same as the circular nozzles. In general, the slot nozzle gives higher speeds in the jet flow. This can be explained by the fact that there are less friction forces on the slot. The total area of the slot is similar to the circles, but the circumferential length is less. Therefore more friction will be present

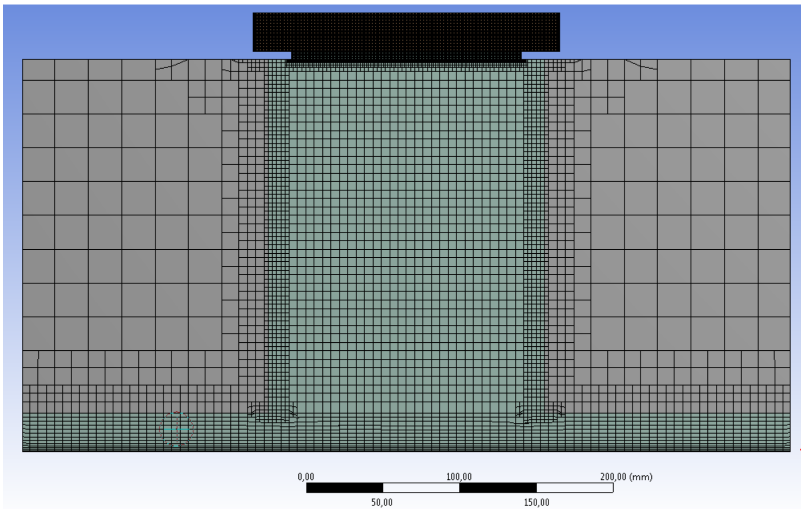

Figure 4.8: Top-view cross-section slot nozzle mesh

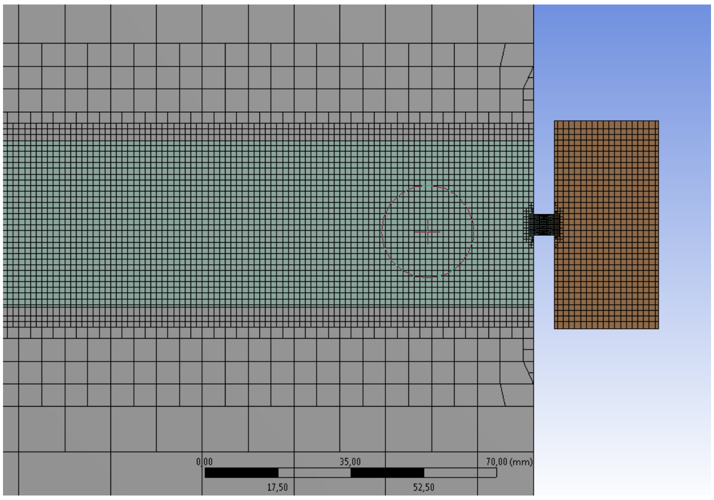

Figure 4.9: Side-view cross-section slot nozzle mesh

in the circular nozzles. Further, the flow also becomes more narrow towards the wall which gives it a smaller imprint on the impinging wall. To make a better assessment of velocity magnitude and jet width, in the next section velocity profiles are setup representing different distances to the nozzle.

The kinetic turbulence energy graph show very different results, but this was high expected. The $k-\epsilon$ scalable WF model and $k-\omega$ SST model do not induce any regions with excessive turbulence. In the $k-\epsilon$ enhanced WT model, the wall region does show very high turbulent kinetic energy. The writer could not explain the origin of this. From experience with other models, the occurrence of this phenomena is not likely to happen in the full scale model.

The heat flux and temperature contour plots all give predictable results. Because of the higher flow rates, the heat flux and temperatures will be higher. Note that the heat flux contour has a different scale. The contours have similar shapes to the circular nozzles. The main difference are the 2 circular regions in the centre of the heat flux contours, they are closer together because of the more narrow flow. And the magnitude of the heat flux (in these graphs very low, minus 500, represents a large heat flux into the wall) is higher because of the higher velocities on the wall. The shape of the $k-\epsilon$ enhanced model is different because of the bad prediction of turbulence in this model.

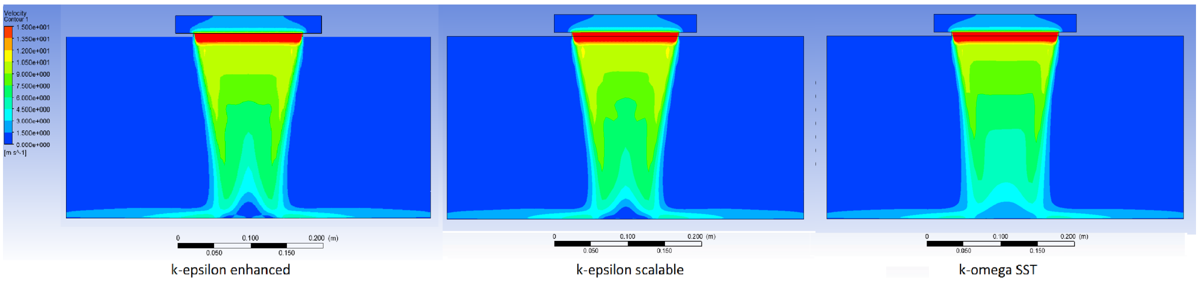

Figure 4.10: Velocity contours of Nozzle slot cross-section

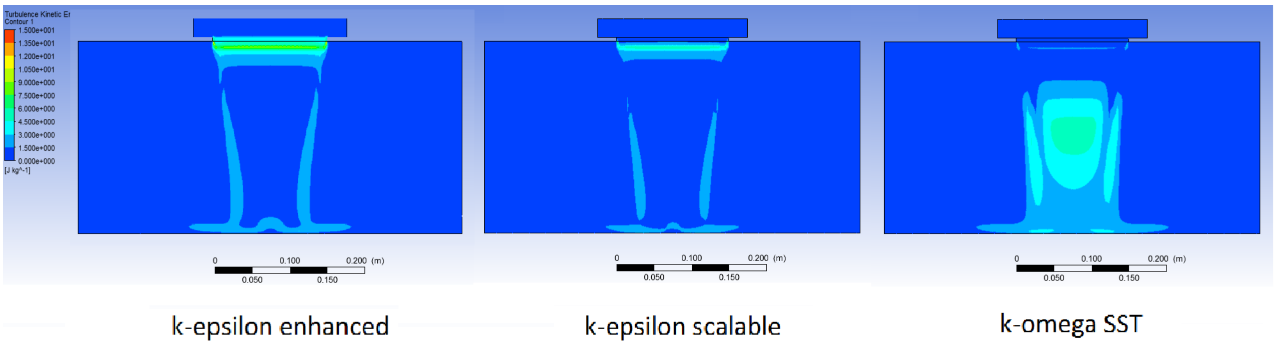

Figure 4.11: Turbulence intensity at Nozzle slot cross-section

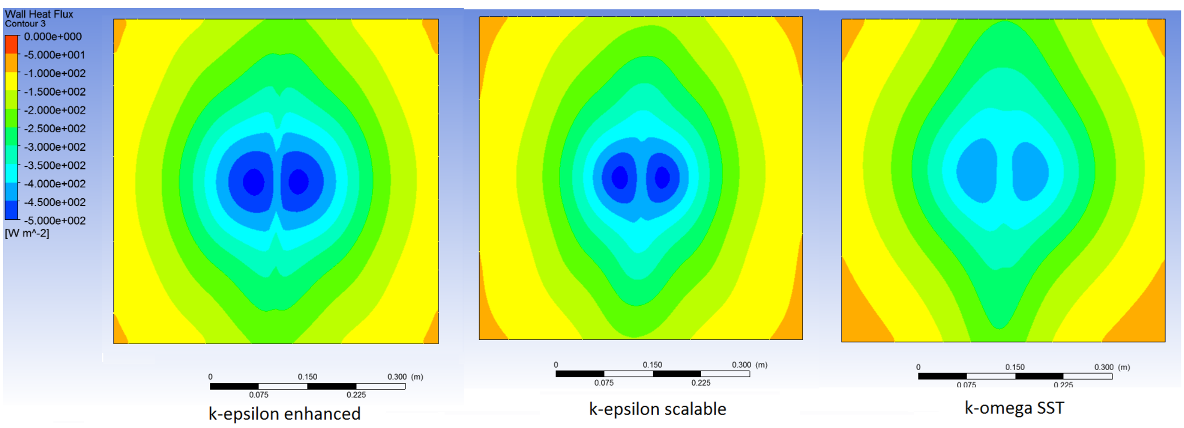

Figure 4.12: Heat flux contours on impinging wall

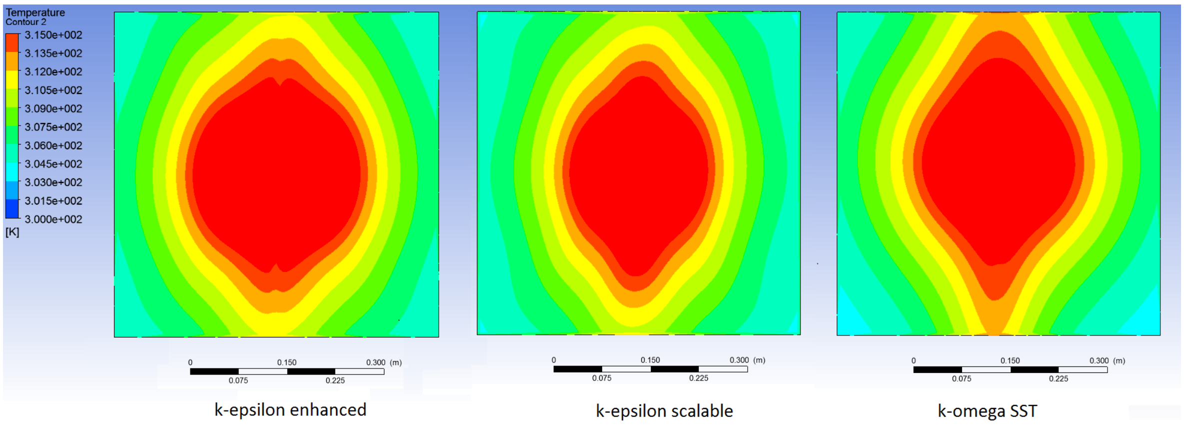

Figure 4.13: Temperature contours of impinging wall

4.1.3 Slot jet correction

To compare the slot flow with the 8 circular jets, the velocity profiles at $z/D = 5$, $z/D = 10$ and $z/D = 15$ are plotted. See graphs 4.14,4.15. In the region near the nozzle, within the jet core length of $z/D = 5$, there is a significant difference in velocity profile. At distances larger then $z/D = 10$ the jets blend in to 1 main flow. From here and further downstream, the flow is very similar to a flow from the slot orifice. A difference between the flows are the velocity amplitudes. The average throughput of the nozzle with the slot is higher comparing to the nozzle with circular jets.

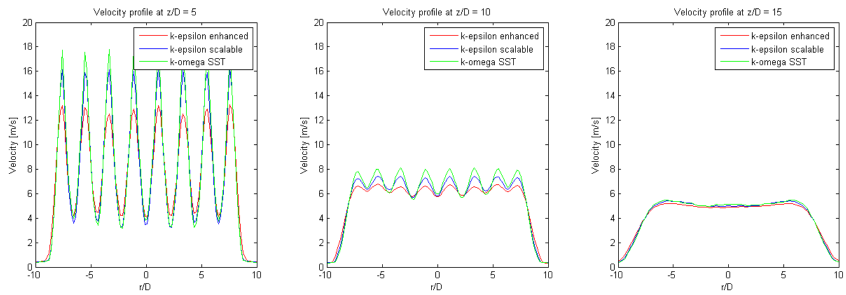

Figure 4.14: Velocity profiles of circular jet nozzle

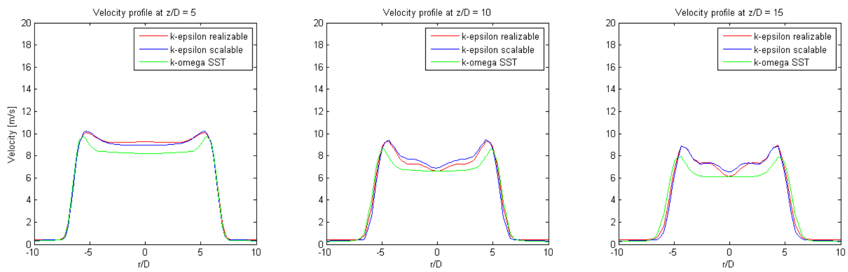

Figure 4.15: Velocity profiles of slot nozzle

From fluent is calculated that the slot nozzle has a inlet mass flow of 0.012 kg/s and the circular jet nozzle 0.009 kg/s.This deviation can be explained by the fact that the circular nozzles have more wall friction losses comparing to the slot. A simple solution is used to counteract this: we can say for an incompressible flow that the pressure difference scales quadratic with the velocity. Since the mass flow rate difference for this case is ≈ 20% lower, the inlet pressure is lowered from 200Pa to 130Pa. These flows are represented by the profiles shown in 4.16, who are, after a distance $z/D = 10$ very comparable to the circular velocity profiles.

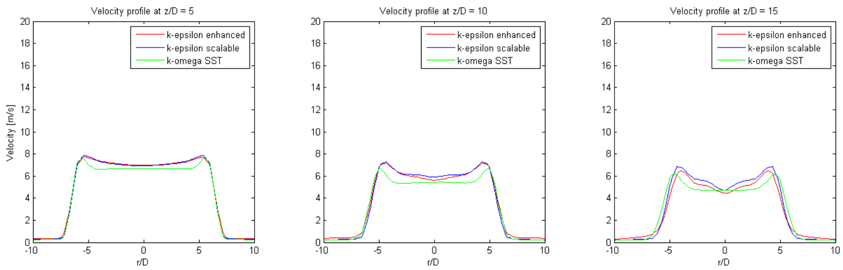

Figure 4.16: Velocity profiles of slot nozzle with adjusted inlet pressure

4.1.4 Conclusion

Modelling the "C-nozzles" as 8 circular jets with diameter 10mm is feasible with the Circular nozzle model shown in this section. Because of its circular shapes it needs a high amount of mesh elements, which makes it not usable for a full scale model where 20 nozzles need to be simulated. For this, a slot shaped nozzle is proposed which only has a full rectangular geometry. This lowers its element amount with 40% making it better usable for a full scale model. The implications are that the flow's velocity profiles are not exactly similar to the real "C-nozzle" case. The magnitude of the velocity is higher, which can be easily corrected by adjusting the pressure settings. The turbulence intensity was expected to be different, but this has a low impact on the shapes of the heat flux and temperature contours.

For further setting up a full scale model, there is not 1 turbulence model that seems to be better. The $k - \epsilon$ scalable WF model will have the advantage that the mesh near the bottle-wall can be coarse. But from the small scale models, its performance could hardly be proven. The $k - \epsilon$ enhanced model and $k - \omega$ SST model both seem effective. Since the $k - \epsilon$ was more often used by my peers during my internship, a further choice is made to use the $k - \epsilon$ enhanced WT model.

4.2 Full scale tunnel model

The full scale model is based on the rough dimensions of the Fuji steam tunnel. The important parts that have influence on the nozzle jet flow and heat transfer such as the nozzle dimensions, distance between nozzles and distance between nozzle and the bottle are accurately dimensioned with the goal of validating the model. See figure 4.17 showing a sketch of the full tunnel geometry and a side-view and top view in figures 4.18 and 4.19. The mesh is setup with the learnings from the above sections. The geometry of the nozzles is taken as a slot as shown in the former section, because of its decreased amount of mesh elements and gives the ability to use cartesian mesh shapes which makes the sum more stable.

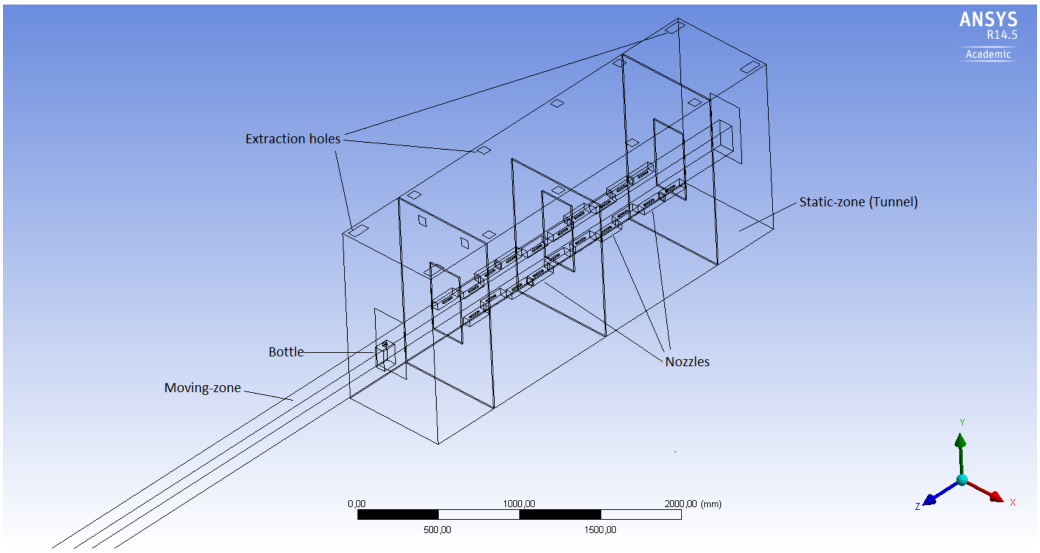

Figure 4.17: Full scale model

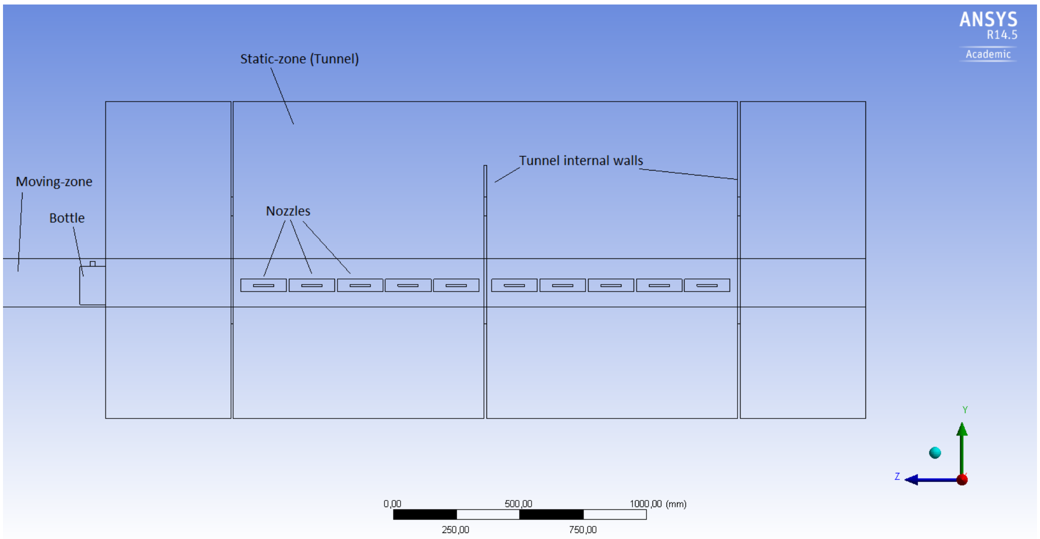

Figure 4.18: Full scale model: side-view

A couple of new objects are introduced in this model. 1) Since the zone where fluid flows is enclosed with walls, their properties also start to play a roll. For simplicity, the walls of the tunnel are modeled as adiabatic walls. Since they only will have a small influence on the heat loss of the tunnel, this can be neglected. The entrance and exit doors for the bottles in the tunnel are modeled as zero pressure areas in the walls. In case of an over-pressure inside the tunnel, the flow will be pushed out of the tunnel through these surfaces. In case of an under-pressure, the doors will supply the tunnel of 293.15K (room temperature) air.

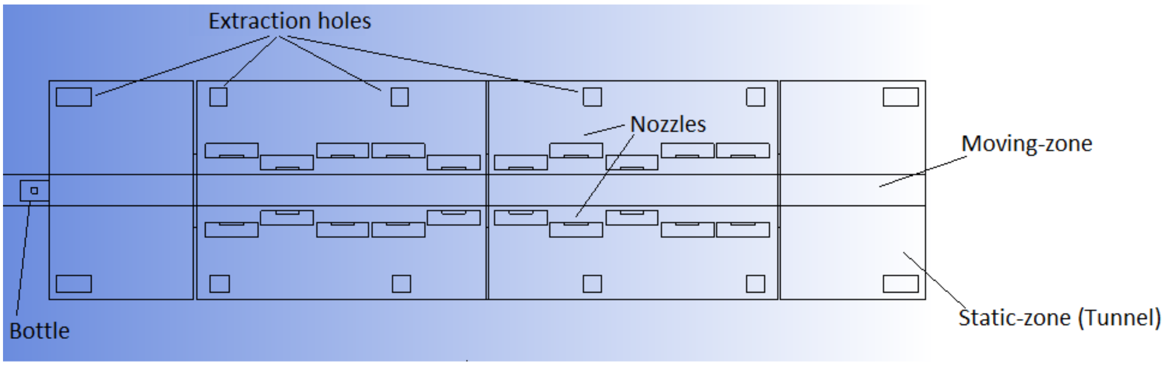

Figure 4.19: Full scale model: top-view

2) Extraction holes in the top of the tunnel are simulated as negative pressure outlets. From measurements with an anemometer the flow speeds of the different holes were examined. With Bernouilli's law, an estimate was made for the pressure boundary conditions of the of the extraction holes.

3) One of the changes that has an high impact on the model is the movement of the bottle through the tunnel. In real life the bottle travels on a conveyor belt through the tunnel. In the model, the conveyor belt is not present. Since it would make the geometry much more complex and since it does not have a big influence on the nozzle flow or heat transfer to the bottle, it is not modelled. The bottle movements is modelled with a sliding mesh that translates through the tunnel geometry with a fixed speed. More about the sliding mesh will be explained in the next subsection.

The turbulence in the flow is modelled with the $k - \epsilon$ realisable model together with the enhanced wall treatment, as said in the former section. Because the enhanced wall treatment is used, the mesh around the bottle needs to be suffice to a boundary layer with $y^+ \approx 1$. Therefore the walls of the bottle get an inflation mesh with first layer thickness of 0.1mm. The mesh of the nozzles is a copy of the nozzle-slot mesh in the former section. See graph fig4.20.

4.2.1 Sliding mesh

To create the ability for the model to show the real movement of a bottle through the tunnel, a sliding mesh was setup. 2 mesh-zones are modeled that represent 1)the static zone which is the tunnel and 2) the moving zone that is the bottle with its surrounding fluid-zone. See figure 4.17. The bottle itself is modelled as a cut-away of the fluid-zone. The surfaces between the cut-out and the mesh are then defined as walls with the properties of PET, similarly as in the former models. The interface between the static zone and moving zone need careful modelling to prevent them from inducing errors in the solution.

In-between the interfaces, the data will be interpolated between the mesh elements. This makes sure that when there are non-conformal mesh nodes, which is very likely for the sliding

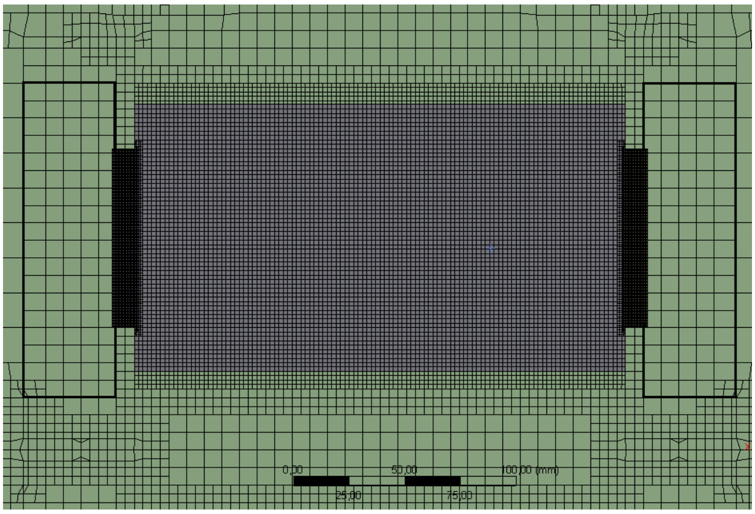

Figure 4.20: Full scale model: Nozzle mesh

meshes, the data is transfered between the 2 zones with this interpolation. When mesh interfaces are conform and when element sizes are small, better results are calculated with the interpolation. When the zones slide next to each-other during a time-step of the moving mesh, the basic rule is that it can only move 1 element size. This allows the interpolation function to work more properly. The small element size needed and the fact that only 1 element size per time-step can be taken, makes that for an accurate solution a high amount of time steps will be needed

As said before, the turbulence kinetic energy and the momentum of the flow are the 2 factors influencing the results of the model the most. To show the influence of the interface on the results, these 2 variables are shown in graphs 4.21 and 4.22 for 3 different interface mesh sizes. From left to right they represent a mesh size of 10mm, 5mm and 3 mm. The interface is shown by the red-line. As can be seen, a clear discontinuity at the location of the interface is seen. Especially in the turbulence kinetic energy plots contours can be seen that the flow is starting to be accurate at 3mm mesh size. In the mesh of the final model, a mesh size of 2mm is taken in the region of the bottle to make sure that the flow is correctly solved around the bottle.

4.2.2 Results

The analysis of the results will be focused on the flow around the bottle. The interaction of the flow with the nozzle is shown in velocity contours and turbulence kinetic energy contours in the region of the bottle, see graphs 4.23,4.24,4.25 and 4.26 The contours are plotted through the centre axis of the nozzle with a cross-sectional view from the top and side. The overall shape of the velocity and turbulence kinetic energy profiles are comparable to the flow fields presented in the "Nozzle model" section.

The goal of the thesis was to understand the temperature seen by the bottle while traveling

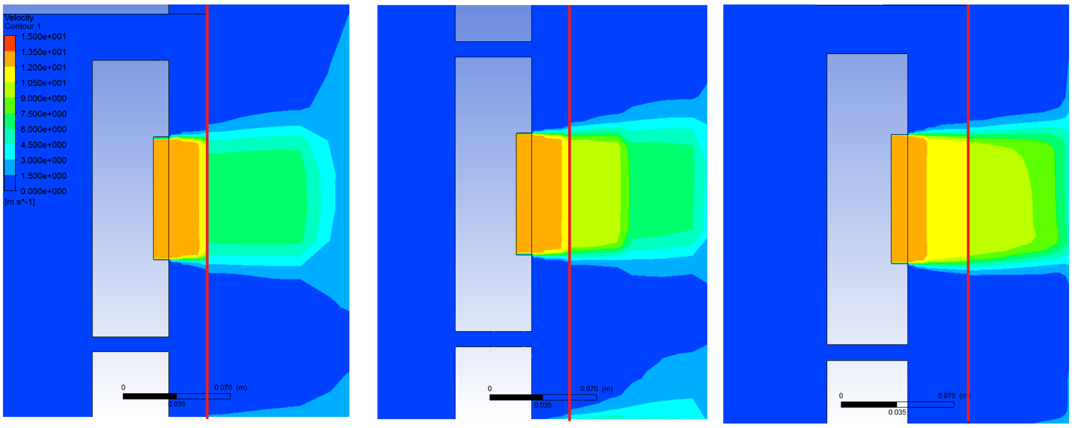

Interface mesh size 10mm Interface mesh size 5 mm Interface mesh size 3 mm

Figure 4.21: Interface: velocity contours

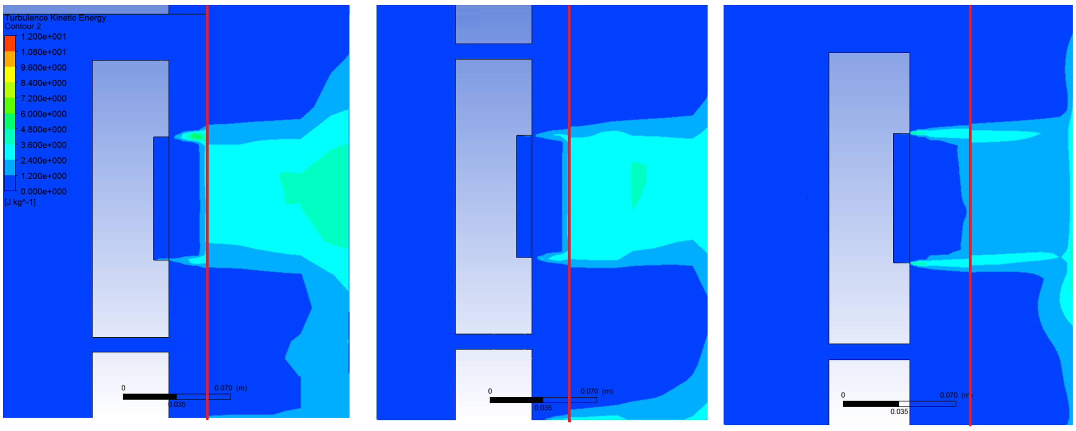

Interface mesh size 10mm Interface mesh size 5 mm Interface mesh size 3 mm

Figure 4.22: Interface: turbulence kinetic energy contours

through the tunnel. The bottle was modelled as a 0.5 mm PET wall with heat properties representing free convective heat transfer of air at the inside of the bottle. 4 examples of temperature profiles are shown. They represent a bottle next to a nozzle with a distance of 30 mm and 70mm between the nozzle outlet and the surface of the bottle. The first 2 nozzles have a jet velocity of 2m/s and the second 2 bottles a jet velocity of 3,5m/s. The bottle in a flow of 2m/s and at 70mm distance shows a maximum temperature of 343K at the flow stagnation region, see figure 4.27. The bottle in a flow of 2m/s and at 30mm distance shows a maximum temperature of 347K at the flow stagnation region, see figure 4.28. The bottle in a flow of 3,5m/s and at 70mm distance shows a maximum temperature of 342K at the flow stagnation region, see figure 4.29. The bottle in a flow of 3,5m/s and at 30mm distance shows a maximum temperature of 355K at the flow stagnation region, see figure 4.30. The difference in flow velocity does not seem to have a big impact on the temperature of the bottle. The distance between the bottle and the nozzle outlet does have a significant difference of

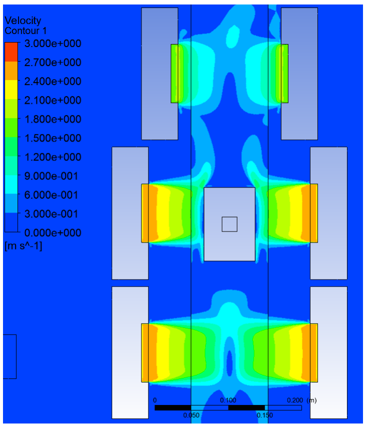

Figure 4.23: Full tunnel velocity profile top cross-section

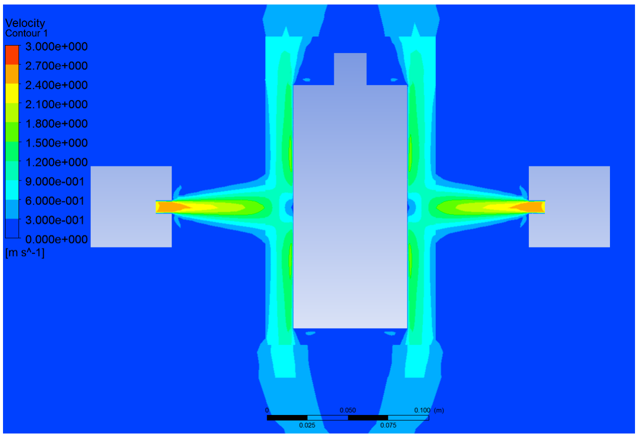

Figure 4.24: Full tunnel velocity profile top cross-section

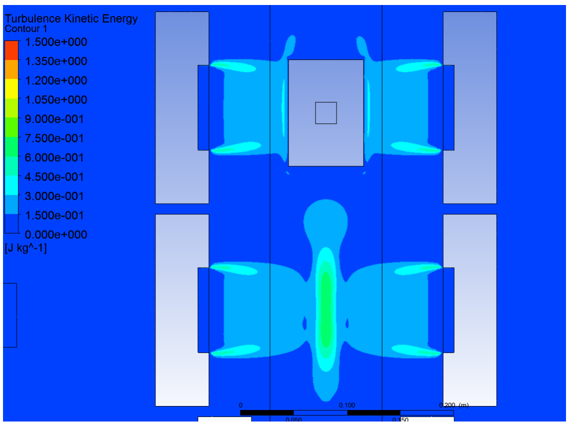

Figure 4.25: Full tunnel velocity profile top cross-section

approximately 10K in the stagnation region on the bottle. Especially in the higher velocity examples, a significant difference can be seen.

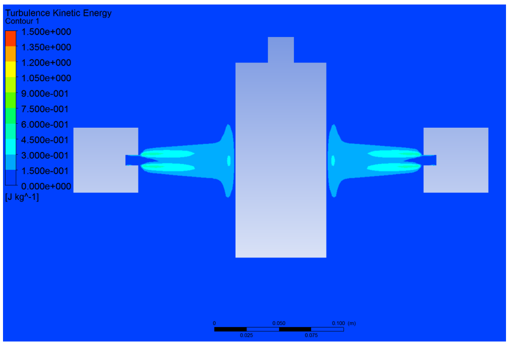

Figure 4.26: Full tunnel velocity profile top cross-section

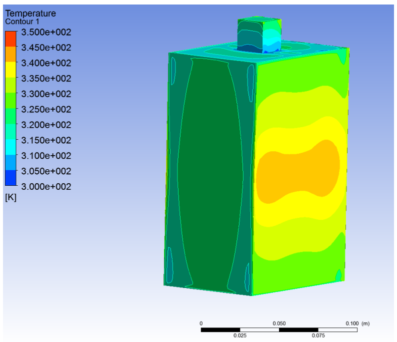

Figure 4.27: Full tunnel Bottle temperature with nozzle at 70 mm, 2m/s

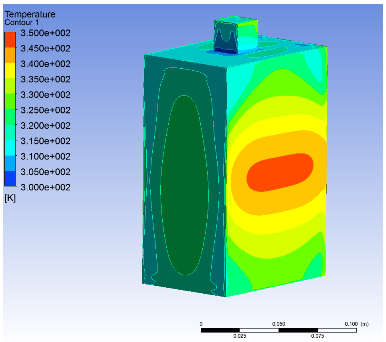

Figure 4.28: Full tunnel Bottle temperature with nozzle at 30 mm, 2 m/s

To show the transient temperatures for the bottle travelling in the tunnel, a graph is made that represents the fluid temperature at the height of the nozzles. The figures are made with a steady-state model, plotting the temperature at the bottle wall position over the length of the tunnel. See figures 4.31, 4.32 and 4.31. The experimental measurements in the next section will show similar graphs, so these results are an excellent reference for the validation of the model. The 3 data sets used for the graphs below are 3 test-setups that were used during experiments.

To explain the data-sets, a short introduction in the experiments should be given: during the experiments, 40 set of measurements are done with all randomly changing settings. 2 of

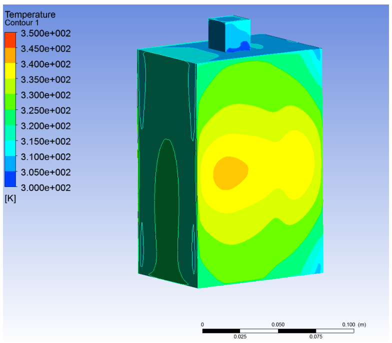

Figure 4.29: Full tunnel Bottle temperature with nozzle at 70 mm, 3.5m/s

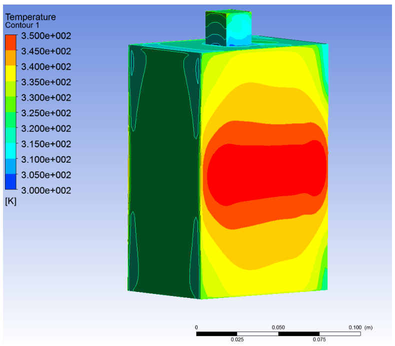

Figure 4.30: Full tunnel Bottle temperature with nozzle at 30 mm, 3.5m/s

the random settings and 1 "repeat" measurements that has all intermediate settings are used in the validation chapter. These 3 settings (also called data-sets) were setup in the model and plotted below. Data-set 1 and 2 are random settings, data set 3 is the settings will an intermediate values.

In this model and in the experiments all nozzles have the same geometrical properties and the extraction fan strength is constant. The variables in this case are 1)the distance between the bottle surface and the nozzle and 2)the flow rate through the nozzles. They will be further specified in the experiments section. From these results can be concluded that the model gives a good overall view of the temperatures. The outside temperature of 27 degC and the upper temperatures of around 90 to 100 deg C are respected. The influence of single nozzles, represented by peaks in temperature, can easily be seen. For further comparison, please read further in the chapter about validation of the model.

The results of this full scale model are based on the steam tunnel of P&G's supplier Fuji Seal. This was chosen because validation measurements could be done on this particular steam tunnel. Since the modelling basis for all different shrink sleeve tunnel dimensions and for different bottle shapes will stay the same, we can say that this still is a generalised research that can be broadly applied. The only changes needed are geometrical updates, the mesh should be detailed according the new geometry and the inlet and outlet boundary conditions should be recalculated.

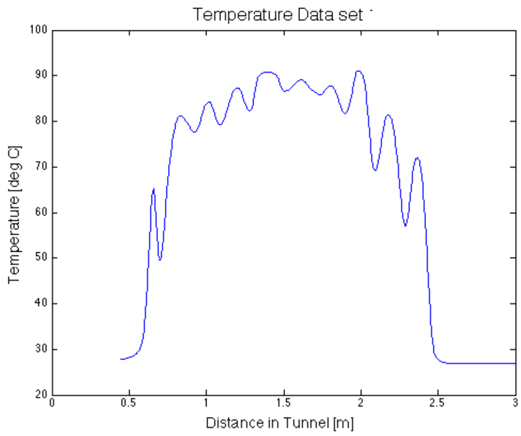

Figure 4.31: Full tunnel Transient temperature for data set 1

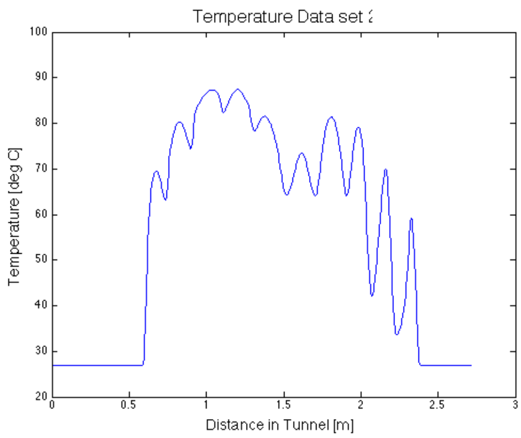

Figure 4.32: Full tunnel Transient temperature for data set 2

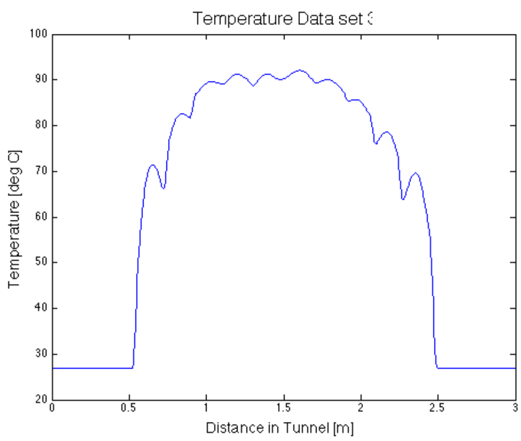

Figure 4.33: Full tunnel Transient temperature for data set 3

Chapter 5

Experiments

Next to the numerical work, also an experimental part has been performed and was an integrated part of the thesis. At P&G's supplier for Shrink Sleeve Labellers Fuji Seal, a test setup was build and 3 days of testing for this thesis were performed. The setup was designed for understanding the steam flow in the steam supply system that brings the steam from the boiler, through a branching system, to the nozzles. Further also a test apparatus was designed to measure temperatures inside the tunnel to understand what temperatures a bottle sees.

5.1 Goal

The goals of the experiment were: 1) Defining the inlet conditions of the steam when it enters the tunnel.These are needed as input data for the CFD model. 2) Collecting data to validate the computational results.

To get an understanding of the steam properties and flow conditions, measurements are done to determine the gauge pressures and temperatures inside the nozzle. The pressure will give an insight in the mass flow per nozzle and the temperature will help understanding the saturation level of the steam. At the inlet of the steam supply system a flow rate meter was installed that shows the instantaneous mass flow rate. The extraction holes on the top side of the tunnel where examined with a hand held anemometer. The measurement setup and processing of the results are shown in the upcoming sections.

For validating the computational results, the goal was too measure "the heat that a bottle sees when it travels through the tunnel". Since the tunnel is setup with many different ways to regulate the flow and its heat transfer to the bottle, it is not easy to understand what the bottle actually undergoes. The goal of the CFD-model is to give insights in this, but for this we also need to measure the influences of the flow on the bottle as a validation. The solution for this was a self-developed measurement tool, named a "SMART-bottle" for its remarkable capabilities comparing to other bottles. More about the specific follow in the next section.

With the above goals, the input details of the model and the validation are covered. Since the measurements were done within a bigger testplan, which was setup for a total understanding of the Shrink Sleeve Setup, the measurements were focused on understanding the bigger picture. E.g. many measurements with the SMART-bottle are done on settings specifically setup for shrinking sleeving a certain type of bottle. For this, 3 types of nozzles with all different nozzle heights, angles, distance to the bottle and pressure settings were setup on the tunnel. To get more suitable data for validation of the model, a specific set of measurements were done. These were held with all A-nozzles, only the nozzle distance to bottle and the pressure settings as variables. A full design of experiments was setup to find correlations between the settings (its internal link) and the heat seen by the bottle.

5.2 Tunnel measurement setup

To measure the temperature inside the steam supply system and inside the nozzles, thermocouples type K are used. They are connected to a data-logger that measures with a frequency of 1Hz. The specific thermocouples have an accuracy of 1deg C. The pressure in the nozzles where measured with differential pressure transmitters who are calibrated between 0 and 7000Pa. The transmitters where coupled with the same data-logger as the thermocouples and also measures with a frequency of 1Hz. See figure 5.1 for the full setup and fig. 5.2 for a detailed measurement nozzle.

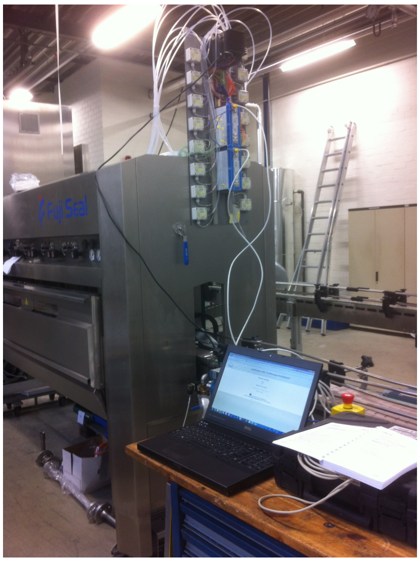

Figure 5.1: Steam tunnel with pressure transducers and datalogger

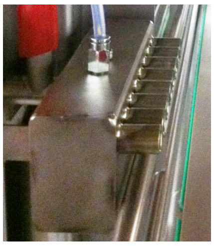

Figure 5.2: Nozzle with tube to pressure sensor and thermocouple

5.3 SMART-Bottle ©

To measure the temperatures seen by a bottle when it travel through the tunnel, a specialised tool was developed. The goal was to understand the transient temperatures of the bottle when being exposed to the steam flows from the nozzles. The ultimate goal would be to measure the heat transport from the flow to the bottle. Possibilities are to measure these with heat flux sensors or hot film sensors. The more simple version would be to measure only temperature with a thermocouple. The estimated temperatures to be measured are between room temperature, 20 deg C, and 110 degC of the steam. Heat fluxes can go up to $5000W/m^2$.

The bottles travel with speeds between $15m/min$ and $70m/min$ through the tunnel. The nozzles have a width of 200mm, so they pass by within $0.6sec$ - $0.2sec$. Therefore the response time should be low enough to give good resolution for the measurements. Heat flux sensors where not able to achieve a low enough time response. Hot films sensors where found to be too complex. Simple K-type thermocouples with wire sizes of 0.125mm where found to have response times of around 0.05 sec for forced convective flows. Since the goal was to understand the transient temperature changes, the response rate is was a hard requirement.

Data logging needed to be done onboard of the tool for which wireless thermocouple nodes were used. With a synchronised 8hz sampling rate, they are not fast enough for the higher-end speeds. For the $15m/min$ - $50m/min$, this sampling rates makes sure there are between 7 and 2 measurements per nozzle.

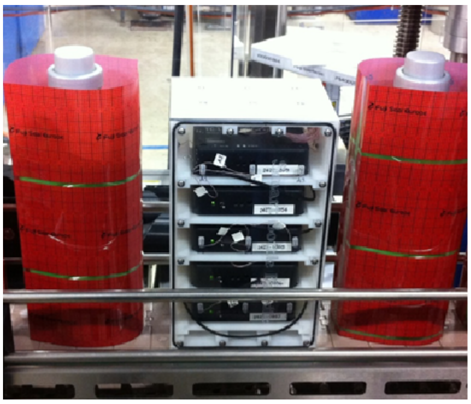

Figure 5.3: SMART-bottle

Figure 5.4: SMART-bottle drawings

5.4 Data and results

Data coming from the thermocouples and pressure sensors were expected to be straightforward relations between tunnel-settings and measurements. Opening a valve was expected to increase the pressure inside the nozzle, resulting in higher temperature of the steam because of the pressure change and increasing the flow rate through the system. Measurements showed that this was not true. The piping system of the steam supply is built up with a combination of serial and parallel connections. See fig. 5.5. Since the control of the steam is performed with manual valves on many different places in the steam supply, it was very hard to understand their response on the flow in the tunnel. E.g. if the valve connected to the first set of nozzles was opened it's pressure would rise, but the pressure in nozzles sets 2, 3 and 4 was lowered. This can be easily explained by the fact that the resistance for that valve goes down, so the flow goes up. Since there is a more or less constant total flow, this means that the flow through the other nozzles will go down.

All of this was not handy for the predictability of the flows. Therefore it was not possible to setup an exact equation for the relation between the valve settings and the pressure, flow rate and temperature of the steam. To find the input conditions for the CFD model, still an indication needed to be found for these values. What is known from measurements per case are: 1) the total flow rate FR, the differential pressures of the nozzles and the temperature in the nozzles. From the total flow rate and the pressures in the nozzles, the flow rate per nozzle is derived. To quickly explain: for an incompressible pipe flow we now the simple Bernoulli relation:

$$\frac{1}{2}\rho v^2 + p = cst \tag{5.1}$$

$$\frac{1}{2}\rho \frac{Q^2}{A^2} + p = cst \tag{5.2}$$

$$\frac{1}{2}\rho\Delta\left(\frac{Q^2}{A^2}\right) = \Delta p \tag{5.3}$$

$$Q^2 = C_v\Delta p \tag{5.4}$$

C_v is the "flow coefficient" of the valves, which is the number representing the friction losses from the valve-setting, nozzles, pipes, bends etc. Because not all data was still availble at the time of writing this part of the thesis, the origin of the exact values can not be shown. The C_v values were calculate by plotting the flow rate and pressure over the valve and nozzle for small flow rate steps over the valve. With the above relation 5.4 C_v was determined for the different valve settings used during the SMART-bottle measurements.

The outcome is shown in an example based on 2 SMART-bottle measurement cases. They are similar to the 2 data-sets represented in the "Full tunnel model" section. The calculated flow rate of per nozzle is shown in a bar chart, see graph 5.6. The specific flow rate for each nozzle is a result of the valve settings, a schematic is shown in graph 5.5. The largest influence comes from valves 2-3-4 who are connecting the respectively nozzles 1-2-3-4, nozzles 5-6-7 and nozzles 8-9-10. respectively the blue, green and red bars in the charts. For the first measurement case valves 2 and 3 are on a low level and valve 4 is on a high level. This can be seen from the fact that the blue and green flow rates are lower comparing to the red bars. The further variation between nozzles are a result of the valve settings just upstream of each nozzle. For example for the red bars, a variation can be seen between nozzle 8 and nozzles 9 and 10. Further also the relative position of the nozzles to the SMART-bottle are given in chart 5.7. The distance varies between 30mm and 70mm. All these settings should give a difference in how much heat is transferred to the bottle.

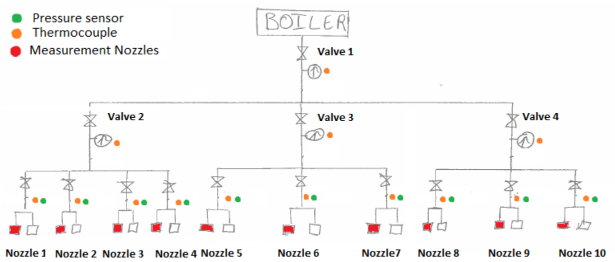

Figure 5.5: Steam supply schematic overview

With the SMART-bottle the temperatures in the flow, similarly as seen by a real bottle, are measured and plotted, see graph 5.8. The data shown is the averaged temperature of 3 thermocouples who are positioned next to each other. The error bars show the standard deviation of the 3 measurement point to give an indication of the repeatability of the measurement. The markers on the blue line show the position of the different nozzles. The data is not very clear, but certain peak at the position of the nozzles can be seen. When trying to find a visual correlation between the flow rate and the temperature, this is not noticeable. A more clear correlation can be seen between the temperature profile and the position of the nozzle. Clear peaks can be seen at nozzle 2 - 5 - 6 and 7. All the nozzles that have the lowest distance between the bottle and the nozzle.

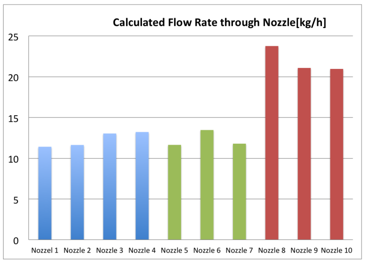

Figure 5.6: Calculated flow rate for each nozzle: data set 1

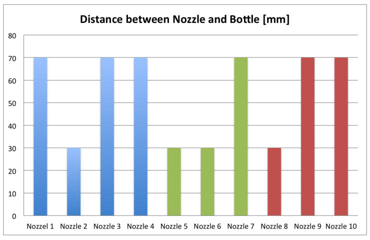

Figure 5.7: Distance between nozzle and bottle for each nozzle: data set 1

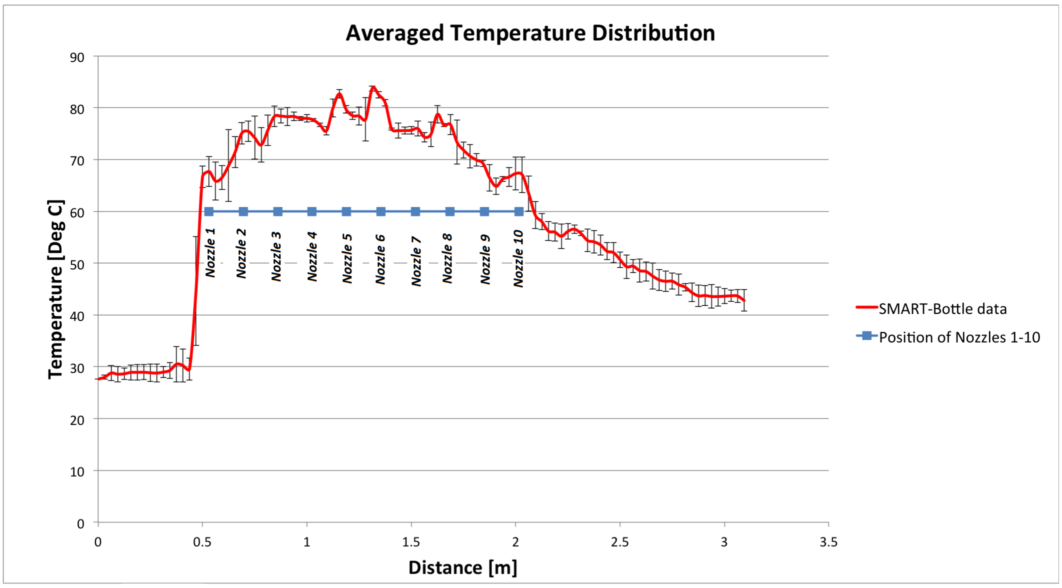

Figure 5.8: SMART-bottle measurements: averaged Temperature data set 1

The second case is setup in the same way. From the flow rate bar chart 5.9 can be seen that the first set of nozzles, have a large flow rate and the nozzles 5 to 10 a relative low flow rate. Again the distance with the bottle is represented by the bar chart 5.10. The combination of these results in a temperature on the bottle which is measured with the SMART-bottle. It's data is shown in figure 5.11. Also in this case their is a more clear correlation between the distance of the nozzle with the bottle and the temperature then between the flow rate and the temperature.

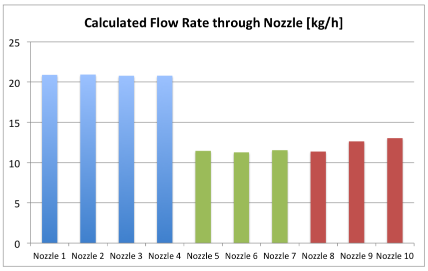

Figure 5.9: Calculated flow rate for each nozzle: data set 2

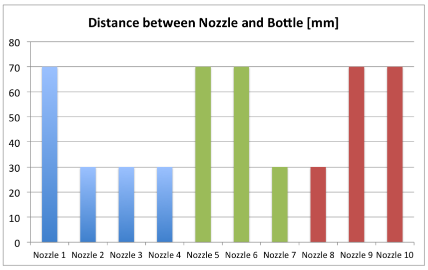

Figure 5.10: Distance between nozzle and bottle for each nozzle: data set 2

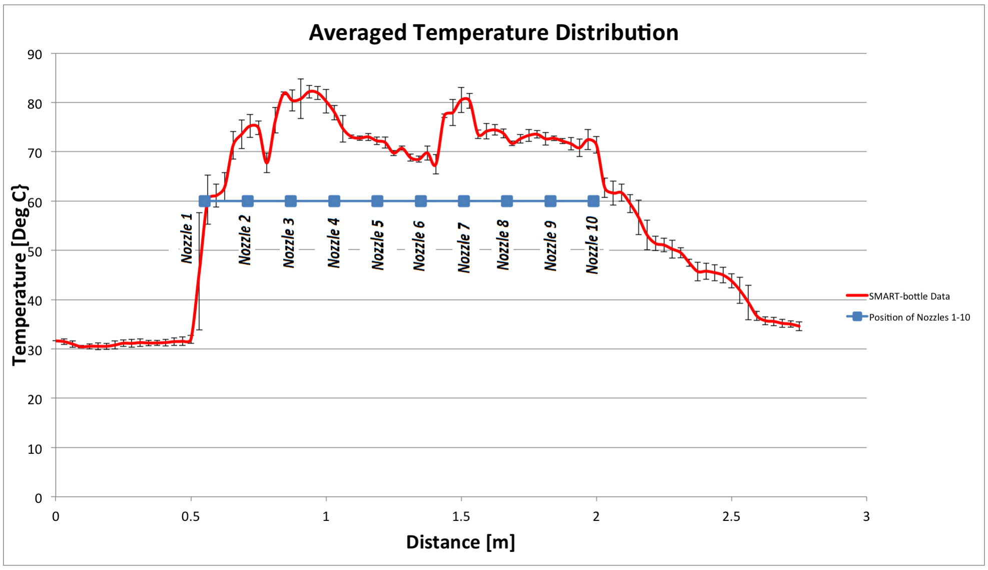

Figure 5.11: SMART-bottle measurements: averaged Temperature data set 2

Finally the third case is a setup where all valve settings are the same and therefor the flow rates are the same, see fig. 5.12. Also the distances between the nozzle and the bottle are the same for each nozzle, see fig. 5.13. It results in a much more smooth temperature measurements, see fig. 5.14. It shows the that the first nozzles only heat the flow to 80 - 85 deg C, the middle section to 90deg C and the last section again to 80- 85 deg C. This shows that the conveyor inlet and outlet cool down the front and aft section of the tunnel. Since the distances and flow rates are all the same, no real correlation can be found between the nozzle positions and the fluctuations in the flow.

The starting temperature of 38 deg C and the temperature of 60 deg C after the tunnel can be explained by the fact that measurements were done very fast after each other. The water condensate that stays on the sensors will show a deviation with the actual temperature seen by the tunnel. In the region where nozzles blow on the bottle, the condensate is blown away, therefore these measurements are believed to be correct. The starting temperature of 38 deg C is a result of the heating of the bottle while doing many experiments in a short time. The bottle was designed of a plastic material because of its low thermal conductivity. Non the less the bottle heats up during many runs inside the steam tunnel.

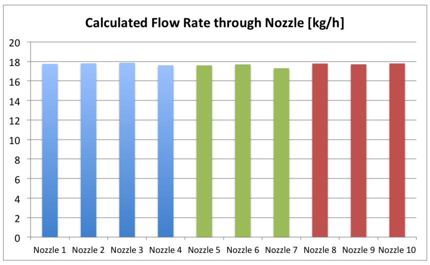

Figure 5.12: Calculated flow rate for each nozzle: data set 3

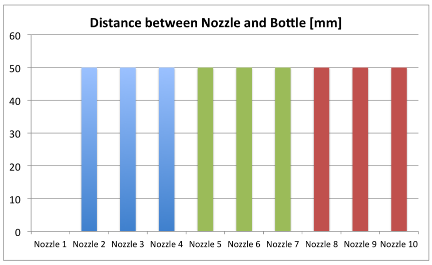

Figure 5.13: Distance between nozzle and bottle for each nozzle: data set 3

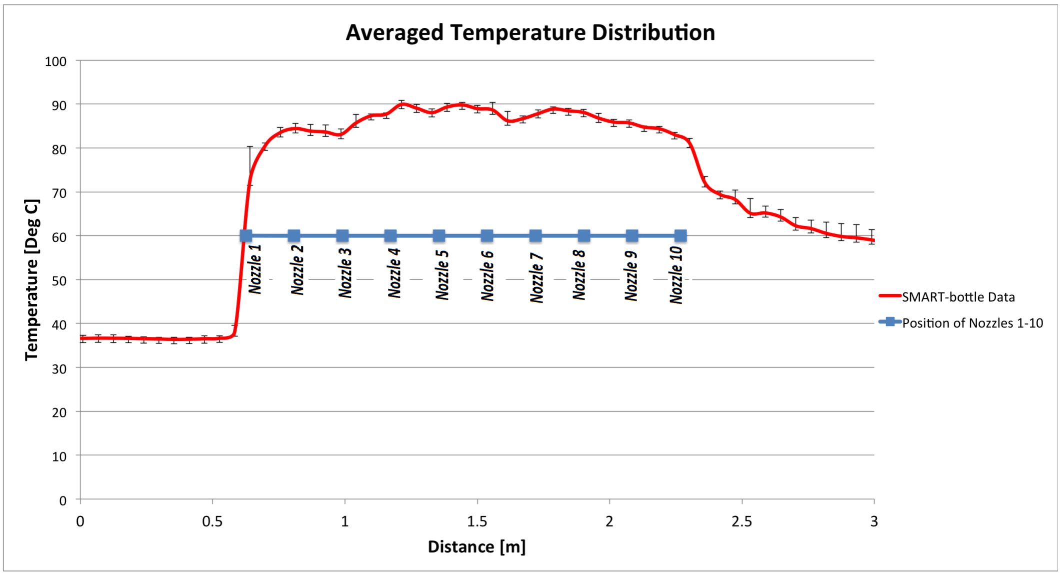

Figure 5.14: SMART-bottle measurements: averaged Temperature data set 3

Chapter 6

Validation

To perform a check on the accuracy of the model, a comparison will be made between the 2 formerly mentioned measurement cases who were performed with the SMART-bottle and 2 simulations done with the CFD-model. The simulation's settings are based on the experiment setups, see table below. Each cases needs a specific mesh which includes the geometrical difference, read distance from bottle to nozzle. The boundary conditions of the model are setup with the measurements from the experiment. Since the temperature of the steam only slightly various from 100 DegC, all nozzle inlets are boundary conditions are 372.15K. The velocities are based on the pressure measurements done during the experiment. From the pressures, the flow rate is calculated per nozzle, see chapter "Experiment" for more details. The outlet pressures are also representable to the real conditions.

Inlet velocity	between 1.4 and 2.4	[m/s]
Outlet gauge pressure	between -5 and -35	[Pa]
Inlet Temperature (100 DegC)	372.15	[K]
Fluid material properties	Air	[-]
Impinging wall k	20	[-] based on free convection of air
impinging wall thickness	0.0005	[mm] Based on PET bottle thickness
Impinging wall material properties	PET	[-]
Tunnel wall material properties	Adiabatic wall	[-]

A sanity check was done know whether the boundary conditions made sense by comparing the total incoming flow rate of the CFD-model and the flow rate measured at the steam supply system during the experiments. For data-set 1 the measured flow rate is 133.9 kg/h and in fluent it was calculated to be 141.5kg/s. For data-set 2 the measured flow rate is 97.45kg/h and in fluent it was calculated to be 101.2kg/h . This shows that the boundary conditions of the model are slightly overestimated but will be representable for the experimental cases.

The "measurement" in the simulation is done with 1 bottle running with a velocity of 15m/s through the tunnel. With fluent, the temperature seen by the bottle is plotted as the fluid temperature at the height of the nozzles vs distance plot. The distance is based on the travelled distance by the bottle through the tunnel.The measurement with the SMART bottle are presented by the temperature profile measured with the thermocouples at the height of the nozzles. They are overlaid with Matlab in graphs 6.2 and 6.1.

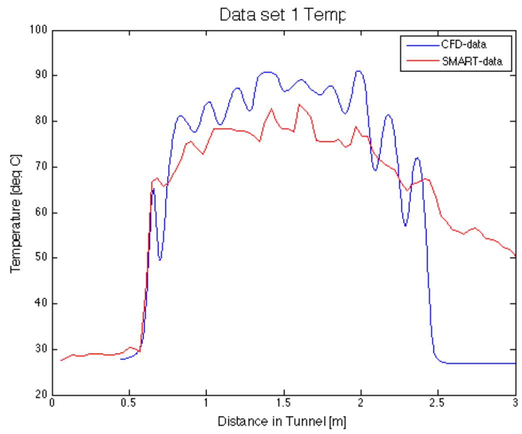

Figure 6.1: Overlay data-set 1

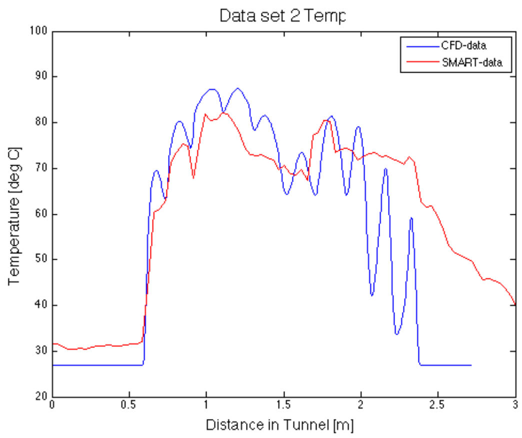

Figure 6.2: Overlay data-set 2

In both cases a clear correlation can be seen between the numerical data and the measured data. At distance 0.7m the tunnel enters the tunnels compartment with nozzles, so the temperature on the bottle rises fast. Further in the tunnel peak are noticeable which are moments where the bottle is next to a nozzle. From distance 2.5 the nozzle leaves the compartment with nozzles, so the temperature drops. The SMART-bottle data stays higher, which is probably the result of residual condensed water on the thermocouples. Especially case 2 shows a clear overall correlation between the simulation and the measurements. An overall error at the peaks of around 5 deg C max is a good result. In data-set 1 there is a more clear deviation of the simulation and the measurements. At the peaks a maximum difference of 10 deg C is still an acceptable result. Finally data-set 3 with all intermediate settings is used as a check, see fig. 6.3

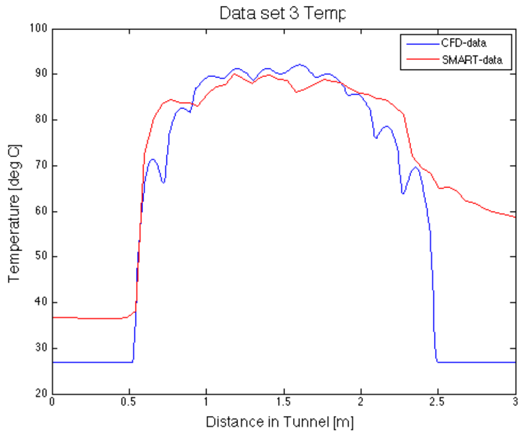

Figure 6.3: Overlay data-set 3

Here the correlation between simulated data and measurements is even more clear. Only the front and aft part of the simulated data is calculated to be lower. The cooling of the conveyor inlet and outlet seems to have a larger effect in the simulation. In the middle section the correlations are very clear and the error is only 2-5 deg C.

6.0.1 Conclusion

As a concluding remark, the measurement data and simulation data are values representing the temperature of the fluid in both cases coming for steady state measurements. The heat transfer between the flow and the bottle, for which a transient simulation is needed, could not be checked and can be the subject for a follow-up research project. Also the fact that condensation is neglected in this case will have a difference on the heat transfer to the bottle. Since the heat capacity of steam and air are relatively close to each other, $1,1 and 1,8 kJ/kgK$, their impact on the total flow temperature and on the forced convection between the flow and wall is expected to be low.

The steady state model shows to be accurate in calculating the temperature of the fluid. Because the sleeve is only 20 - 50 μm thick, often there is assumed that the flow temperature and the sleeve temperature are the same. This makes the current model with its validation already valuable. To be able to get the same confidence in the temperature of the bottle, more validation work is needed as said before.

Chapter 7

Conclusions & Recommendations

The goal of this research was to investigate the heat transfer phenomena in the Shrink Sleeve Labeling process, specifically between the steam flow and the bottle. This investigation was done by developing a numerical tool that predicts the temperatures seen by a bottle when it travels through the steam tunnel. The tool focuses on fundamental understanding of the convective heat transport due to the flow around the bottle. The results were intended to look like an energy or temperature profile on the bottle, showing what the bottle sees under certain settings and circumstances of the tunnel. Since this research was performed at P&G and in collaboration with their supplier, the available data and the facilities used for experiments are focused on "Fuji Seal" shrink sleeve labelling machinery.

7.1 Conclusions

The full scale model is geometrically a representation of the Fuji Seal steam tunnel, but has all the capabilities to also simulate different tunnels with other sizes and shapes. The model is setup with the RANS turbulence model $k - \epsilon$ realisable. This turbulence model was found to be effective for simulating the velocity profiles, turbulence intensity and flow temperatures of the jet flow and wall flow for the shrink sleeve labelling case, which is needed to get a good prediction of the Nusselt number on the wall. The enhanced wall functions were used at the bottle wall since it was found to be most effective in simulating the wall flow and the convective heat transfer between the wall flow and the bottle. A sliding mesh was used to simulate the movement of the bottle through the tunnel. Because the interface needs a relatively small mesh size comparing to the distance the moving mesh needs to travel, it results in computational expensive simulations.

The simulations done with the model are able to predict flow temperature profiles that have good correlations with flow temperature measurements done during experiments. They are accurate with a maximum error between 2 and 10 deg C. For creating fundamental understanding in the Shrink Sleeve Labeling process, this gives confidence in the results and therefore seems to be a sufficient model. The error between the model and measurements can be explained by errors during the measurements and by the assumptions made in the model. The assumptions that have the most impact are: 1) the difference between modelling hot air in the model and steam in the real tunnel. Since no condensation effects are taken into account in the model this will induce an unknown error. 2) A simplification of the nozzle geometry, namely assuming a slot shape instead of circular shaped nozzles, will change especially the turbulence in the flow. 3) Using RANS-models will average out the small scales of turbulence, which makes it less accurate. The $k - \epsilon$ realisable model with enhanced wall treatment was found to have good characteristics for the SSL-tunnel model.

During the experiments, the wall heat flux from the flow to the bottle was not measured, therefore a validation could not be done to check whether the temperature of the bottle was correctly calculated. In the "Jet impingement modelling" chapter a comparison of Nusselt number predictions is made between the simulations and literature, which gives some confidence that the model has the capability of correctly predicting the Nusselt number. If then the boundary conditions of the bottle, represented by a convective wall in fluent, are correctly set the model should be able to predict the heat fluxes and temperature of the bottle itself. For the temperature of the sleeve, it can be said that it will be the same as the temperature of the flow. Because the sleeve is only $50\mu m$ thick, this assumption is often made in the shrink sleeve business. This makes that the current model has the capability to give a direct impact on fundamentally understanding the heat transfer between the flow and the sleeve.

At this moment when a new case or a changed tunnel setting needs to be setup in the model, the geometry of the tunnel needs to be manually adapted which takes approximately 1/2 day of effort. The mesh of the full tunnel counts around 4 million elements, which makes it a computational costly model. Especially when bottle movement was modelled with a 2mm interface cell width, the transient model needs 1500 time steps. Running the full model takes 5 days with 16 CPU cores. This makes it a model that is not versatile for running many cases and therefore less useful for the business.

Some learnings made during the experiments and from the simulations which were found to be interesting for the shrink sleeve labelling business are the following:

- The velocity profile of the nozzle with circular jets will blend together in a uniform flow after 10 nozzle diameters behind the jet exit. The uniform flow will result in a more uniform heat transfer on a bottle comparing to the heat transfer from a flow closer to the nozzle. For shrink sleeve labelling this will make the actual shrinking of the sleeve more predictable.

- The heat transfer from the nozzle with circular jets is very similar to the nozzle with a slot jet. This indicates that the shape of the jets does not seem to influence the heat transfer of the flow to the bottle. Currently, many different nozzle shapes are used in the sleeving tunnels. From measurements we learn that the different shape does influence the flow rate of the flow for a certain pressure. Therefore we can conclude that the shape does influence the heat transfer because it regulates the flow rate, but does not particularly influence the heat transfer because of a different flow characteristics behind the nozzle.

- The flow in the shrink sleeve labelling steam tunnels is currently monitored with pressure sensors at the nozzles. Since the driving variable of the heat transfer is the flow rate, this gives a bad indication of what exactly happens inside the tunnel. Especially since nozzles with different shapes will have different flow coefficients.

7.2 Recommendations

From a modelling and simulation perspective, the goal was the build fundamental understand and a tool that can predict the heat seen by a bottle that runs through the tunnel with different settings. The current numerical tool is not enough versatile to be used for "trying out new bottles and new settings". The computational cost and the need for a complete new geometry and mesh to tryout a new setting will make the effort too intensive in comparison with doing experiments with real bottles at a supplier.

At the other hand, when a new steam tunnel in its conceptual design-phase needs a review, this model can be of purpose. Normally a concept tunnel needs to be built for reviews, but from now on the model can give a large amount of new info before building anything. Although still a full geometry and mesh needs to be drawn, now it could become cost effective since no concept tunnel is needed.

As a next step, the validation of the heat transfer in to the bottle will give a large increase in confidence in the model. At this stage only the flow temperatures are validated, but the model can also predict the heat transfer to the bottle. When the heat transfer part of the model also is validated, the model is fully validated for its purpose. In case the measurements turn out give large deviation from the current model, it is very likely that neglecting the condensation of steam is the origin of the error, so a further investigation in that part of the model should be done.

From a more practical perspective, a couple of recommendations can be given about the steam tunnel used for the validation of the model. As said in the conclusions section, currently the nozzles and their monitoring devices do not fit their purpose, which makes the sleeving process unpredictable and the tunnel settings counter-intuitive. In case a new design of the tunnel will be made, the main focus should be on how the jet flow behind the nozzle looks like and on the control of the flow rate through the nozzles. The goal should be that the flow results in a uniform and controllable heating of the bottle.

During the post-processing of the experiment data, the flow rates were calculated with the flow coefficient of the valves and nozzles, with the pressure and the total flow rate. This could be an intermediate solution to get an estimation of the flow rates per nozzle for different valve settings. A calculation like this was relatively easy in this case since all the nozzles are the same, so their flow coefficient are the same. For setups with many different nozzle types, this will get more complex but is certainly feasible.

Bibliography

G Abramovich and L Schindel. General properties of turbulent jets.

Axon. Example steam tunnel, Axon, 2014. URL http://www.axoncorp.com/news/axon-advances-its-thermopoint-steam-heat-shrink-tunnel-introduces-thermopoi/. Retrieved: 16-10-2014.

JM Beer. Combustion aerodynumics. *Combustion Technology: Some Modern Developments*, page 61, 2012.

M Behnia, S Parneix, and P Durbin. Accurate modeling of impinging jet heat transfer. *Center Turbulence Research Annual Research Briefs*, pages 149–164, 1997.

L Boguslawski and Cz O Popiel. Flow structure of the free round turbulent jet in the initial region. *Journal of Fluid Mechanics*, 90(03):531–539, 1979.

TJ Craft, LJW Graham, and Brian Edward Launder. Impinging jet studies for turbulence model assessmentii. an examination of the performance of four turbulence models. *International Journal of Heat and Mass Transfer*, 36(10):2685–2697, 1993.

Ansys Fluent. 12.0 theory guide. *Ansys Inc*, 5, 2009.

U Heck, U Fritsching, and K Bauckhage. Fluid flow and heat transfer in gas jet quenching of a cylinder. *International Journal of Numerical Methods for Heat & Fluid Flow*, 11(1): 36–49, 2001.

Sleeve Seal Patrick Houston. Example steam tunnel, Sleeve Seal, 2014. URL http://www.sleeveseal.patrickhouston.com/wp-content/uploads/2014/05/SSL-1200pi.pdf. Retrieved: 16-10-2014.

K Jambunathan, E Lai, MA Moss, and BL Button. A review of heat transfer data for single circular jet impingement. *International Journal of Heat and Fluid Flow*, 13(2):106–115, 1992.

X Liu, JH Lienhard, and JS Lombara. Convective heat transfer by impingement of circular liquid jets. *Journal of heat transfer*, 113(3):571–582, 1991.

Franciscus Theodorus Marie Nieuwstadt. *Turbulentie: inleiding in de theorie en toepassingen van turbulente stromingen*. Epsilon, 1992.

Tadhg S ODonovan. Fluid flow and heat transfer of an impinging air jet. *Department of Mechanical and Manufacturing Engineering*, page 145, 2005.

Bengt Sundén, Andreas Abdon. Numerical investigation of impingement heat transfer using linear and nonlinear two-equation turbulence models. *Numerical Heat Transfer: Part A: Applications*, 40(6):563–578, 2001.

Quadrel Labeling Systems. Example steam tunnel, Qadrel Labeling Systems, 2014. URL http://quadrel.com/steam-heat-tunnel.html. Retrieved: 16-10-2014.

L Thielen, HJJ Jonker, and K Hanjalić. Symmetry breaking of flow and heat transfer in multiple impinging jets. *International journal of heat and fluid flow*, 24(4):444–453, 2003.

XS Wang, Z Dagan, and LM Jiji. Heat transfer between a circular free impinging jet and a solid surface with non-uniform wall temperature or wall heat flux2. solution for the boundary layer region. *International journal of heat and mass transfer*, 32(7):1361–1371, 1989.

Frank M White and Isla Corfield. *Viscous fluid flow*, volume 2. McGraw-Hill New York, 1991.

MinYi Xu, JianPeng Zhang, JianChun Mi, GJ Nathan, and Peter Anthony Markus Kalt. Piv measurements of turbulent jets issuing from triangular and circular orifice plates. *Science China Physics, Mechanics and Astronomy*, 56(6):1176–1186, 2013.